Title
ANTINEUTRON PRODUCTION BY CHARGE EXCHANGE

Author
Weingart, Richard C.

Publication Date
1957-10-18

UCRL 8025

UNIVERSITY OF CALIFORNIA

Radiation Laboratory

BERKELEY, CALIFORNIA

DISCLAIMER

UCRL-8025

UNIVERSITY OF CALIFORNIA
Radiation Laboratory
Berkeley, California

Contract No. W-7405-eng-48

ANTINEUTRON PRODUCTION BY CHARGE EXCHANGE

Richard C. Weingart
(Thesis)

October 18, 1957

Printed for the U. S. Atomic Energy Commission

Contents

ANTINEUTRON PRODUCTION BY CHARGE EXCHANGE

Richard C. Weingart

Radiation Laboratory
University of California
Berkeley, California

October 18, 1957

ABSTRACT

Antineutrons produced by 440-Mev antiprotons incident upon Pb, C, and CH_2 targets have been observed. The antineutrons were detected by their energy release upon annihilation. Charge-exchange cross sections for antiprotons in the three targets have been calculated. The cross section for the process $\bar{p} + p \rightarrow \bar{n} + n$ has been obtained from the CH_2 and C data by subtraction. The results show that the effective charge-exchange cross section per proton of the target nucleus decreases rapidly with increasing Z. Calculations based on an optical model for the exchange process in nuclei are found to be consistent with the experimental results for C and Pb.

I. INTRODUCTION

The observation of antiprotons produced in high-energy nucleon-nucleon collisions led to the belief that antineutrons are also created in such processes.[1] The existence of the antineutron has recently been demonstrated by Cork, Lambertson, Piccioni, and Wenzel by utilizing the reaction $\bar{p} + p \rightarrow \bar{n} + n$.[2] The antineutron is characterized by the following fundamental properties: (a) mass equal to that of a neutron, (b) zero charge, (c) lifetime equal to that of a free neutron, (d) fermion of spin 1/2, (e) magnetic moment equal to +1.91 nuclear magnetons, and (f) the ability to annihilate in combination with nucleons with the subsequent release of approximately 2 Bev of energy. Thus to distinguish between the antineutron and neutron, Property (e) or (f) must be demonstrated. Because the antineutron has zero charge, it was not possible to observe this particle by use of a magnetic mass spectrograph similar to that employed in identifying the antiproton.[3]

We have utilized the annihilation property (f), characteristic of antinucleons, to detect the antineutron. For this purpose a counter was constructed in which the annihilation process could be detected. This counter was constructed to satisfy two requirements: first, a large fraction of the 2 Bev of energy released upon antinucleon annihilation must be spent within the counter without any appreciable fraction escaping through its sides; secondly, the response of the counter should be a monotonic function of the energy deposited in it. Antineutrons produced directly by nucleon-nucleon collisions are difficult to detect by this method because of the presence of a very-high-energy neutron background. These neutrons, which extend to 6 Bev in energy, can deposit in the counter energies that are comparable to the annihilation energy. We therefore sought an alternative mode for the production of these particles.

In analogy to the observed n-p charge-exchange scattering, it is reasonable to expect that antiprotons are also capable of undergoing an exchange process with nucleons of ordinary matter, thereby producing a nucleon-antineutron pair. The possible antiproton-nucleon reactions leading to the formation of an antineutron are

(a) with protons,

$$\bar{p} + p \rightarrow \bar{n} + n ,$$

$$\bar{p} + p \rightarrow \bar{n} + n + \pi^0 ,$$

$$\bar{p} + p \rightarrow \bar{n} + p + \pi^- ;$$

(b) with neutrons,

$$\bar{p} + n \rightarrow \bar{n} + n + \pi^- .$$

An order-of-magnitude calculation, based on phase-space arguments, predicts that those processes involving the formation of pions compete poorly with the direct process $\bar{p} + p \rightarrow \bar{n} + n$.* In what follows we consider that charge-exchange antineutrons are formed in proton-antiproton collisions and are unaccompanied by pions. Comparison to n-p charge-exchange scattering leads us to expect that the differential cross section for the antineutron distribution is peaked strongly near 0^o in the laboratory system. Therefore, the region of interest extends from 0^o with respect to the beam direction to some limiting angle determined by the size of our apparatus. The method employed to observe the antineutrons was the following: Antiprotons, certified as to their nature by a system of analyzing magnets and counters, were allowed to strike a target. Large plastic scintillation counters, located in back of this target, were used to distinguish between charged and neutral particles, resulting from antiproton interactions in the target, which were projected into a cone along the beam direction. The antineutron detector mentioned in the preceding paragraph was located farther back along the beam direction and defined the aperture of this cone. Its function was to distinguish between antineutrons and all other neutral particles also arising from antiproton interactions by the energy release of these various particles within this counter. These neutral particles result from antiproton annihilation or scattering in the target, and the energies deposited in the counter by these particles are small in comparison with the 2 Bev of energy release upon antineutron annihilation.

---

*See Appendix I for this calculation.

Utilizing this method of production and detection, we have observed antineutrons produced by 1080-Mev/c antiprotons incident upon Pb, C, and CH_2 targets. Charge-exchange cross sections for these materials have been calculated from the experimental data on the assumption that the attenuation of antineutrons is identical to that of antiprotons. The charge-exchange cross section for antiprotons on free protons has been obtained from the CH_2 and C data by subtraction. The experimental values obtained for C and Pb have been compared with the results of optical-model calculations using the elementary $\overline{p}$-p charge-exchange cross section and the total attenuation cross section for antiprotons on free nucleons. Satisfactory agreement with the experimental results has been obtained for C and Pb by use of a uniform Fermi distribution for the nucleon density.

II. EXPERIMENTAL PROCEDURE

A. The Antiproton Beam

The circulating beam of the Bevatron was spilled onto an internal target over a period of 100 milliseconds near the end of the accelerating cycle of each pulse of the machine. During this time the proton beam energy varied from 5.8 to 6.3 Bev. Antiproton-production targets used were CH_2 and C. A beam of negatively charged particles of momentum 1.19 Bev/c resulting from proton interactions in the target was bent by the fringing field of the Bevatron into the magnetic channel shown in Fig. 1. This beam contained antiprotons and other particles (mostly negative pions) in the ratio of approximately 1:30,000. Upon passing through the first magnet D, the negatively charged beam underwent an additional bending of 3.2° that guided it into the remaining segments of the magnetic channel. The 8-in.-diameter quadrupole focusing lens Q1 focused this beam at the center of the 4-in. quadrupole L. Between lenses Q1 and L was a bending magnet M1 which resulted in a deflection of 14.0° for particles of momentum 1.19 Bev/c. The quadrupole L focused particles from Q1 at the entrance aperture of the last lens Q2. The bending magnet M2 between quadrupoles L and Q2 caused the negative beam to undergo a further bending of 18.8°. Finally Q2 focused the beam at F2. The first part of the magnetic channel, consisting of D, Q1, M1, and L, was tuned to a momentum of 1.19 Bev/c. Ionization losses in a counter located at the exit end of L reduced the momentum of the beam to 1175 Mev/c, therefore the remaining system (M2 and Q2) was tuned for this lower momentum. A description of the apparatus shown in Fig. 1 is given in Table I.

The counters used to distinguish the antiprotons from the large background of other particles of the same momentum were F1, F2, C1, C2, and S1. Their locations relative to the magnetic channel are shown in Fig. 1. F1 and F2 are Cherenkov counters which detect charged particles in the velocity interval $0.65 < \beta < 0.86$. They are of a design originated by Fitch,[4] which utilizes the angle for total internal

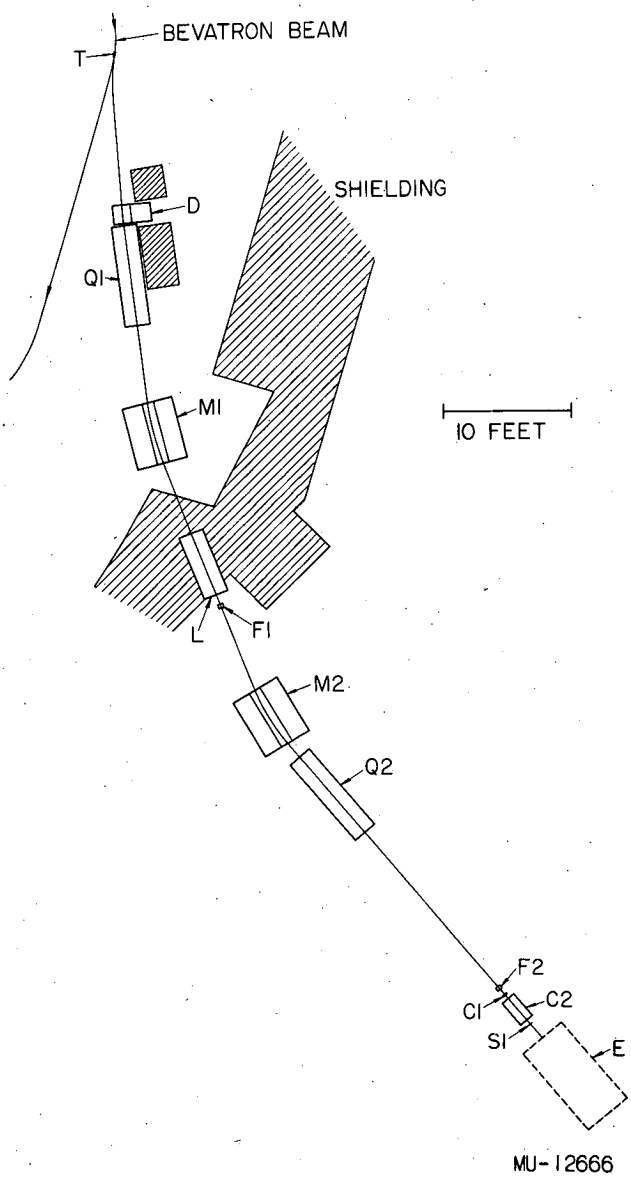

Fig. 1. Schematic drawing of the mass spectrograph that served to identify the antiprotons incident on the area designated by E in this figure.

Table I

Characteristics of components of the apparatus shown in Fig. 1.

T	Bevatron target (production target for antiprotons).
F1	Fitch-type Cherenkov counter of styrene with 2.5% ethyl bromide added: $\mu_D = 1.54$, $\rho = 0.91$ g cm^{-3}; diameter 3.88 in., thickness 2.31 in.
F2	Same as F1 except diameter 2.5 in.
C1	Cherenkov counter of Fluorochemical 0-75 ($C_8F_{16}O$); $\mu_D = 1.276$; $\rho = 1.76$ g cm^{-3}; 4 in. square by 1.5 in. thick.
C2	Cherenkov velocity-selecting counter of lucite; $\mu_D = 1.50$; $\rho = 1.18$ g cm^{-3}; diameter 2.37 in., thickness 4.25 in.
S1	Plastic scintillation counter 4.0 in. in diameter by 0.62 in. thick.
E	Area occupied by apparatus and counters for the production and detection of antineutrons.
D	Deflecting magnet 18 in. long; aperture 12 in. wide by 5 in. high; 3.2° bending.
Q1, Q2	Quadrupole focusing magnets of 8-in. aperture.
M1, M2	Deflecting magnets 60 in. long; aperture 12 in. wide by 7 in. high; 14° bending and 18.8° bending respectively.
L	Quadrupole focusing magnet of 4-in. aperture.

reflection of Cherenkov light emitted by particles with $\beta > 0.86$ so that this light cannot reach the phototube. F1 and F2 were separated by 40 ft, corresponding to an antiproton time of flight between these counters of 51 millimicroseconds. In addition to the requirement that an antiproton must register in both F1 and F2 there is also a requirement for the proper separation in time between pulses from these counters. Counter C1 is a Cherenkov counter that counts charged particles with $\beta > 0.78$. Ionization losses in F1 and F2 reduce the energy of the antiprotons so that they cannot count in C1. C2 is another Cherenkov counter,[5] which counts charged particles only in the narrow velocity interval $0.75 < \beta < 0.78$. The velocity of an antiproton in C2 is given by $\beta = 0.76$. The last counter of the system S1 is a 4-in-diameter plastic scintillation counter defining the beam that was incident on the experimental area designated as E in Fig. 1. The efficiencies of the various counters for rejecting charged particles with β outside the limits given for them are 90% in F1 and F2, and 97% in counter C2. The fact that these efficiencies are not much greater is probably the result of nuclear interaction and scintillations in the Cherenkov radiators of these counters. An antiproton incident on the region E of Fig. 1. was therefore defined electronically by: pulses in both F1 and F2 properly separated in time, no pulse in C1, a pulse in counter C2, and a pulse in S1 (i.e., F1, F2, $\overline{C1}$, C2, S1).

Ionization loses in F1, F2, C1, C2, and S1 reduce the antiproton beam incident upon the region E to a mean energy of 497 Mev. The magnetic channel discussed above defined the momentum of this beam to within ± 4%. This range in momentum corresponds to an uncertainty in the antiproton energy of ± 32 Mev at counter S1. The beam divergence as defined by the 4-in-diameter scintillation counter S1 was $\pm 3^{\circ}$.

B. System for the Detection and Production of Antineutrons

The antiproton beam discussed in the preceding section was incident upon the antineutron production-detection system shown in Fig. 2. Counter S1 is included to show the location of this system relative to the magnetic channel in Fig. 1. Approximately five antiprotons per minute entered this system through the 4-in.-diameter scintillation counter S1.

Counter S1 was the last counter of the antiproton-identifying system. Counter C* in a Cherenkov counter filled with methyl alcohol and slotted as shown to accommodate various targets. Nine RCA 6810 photomultiplier tubes were partially submerged in the alcohol, as shown in the schematic drawing of this counter in Fig. 3. The index of refraction of methyl alcohol at room temperature is 1.33, so that charged particles with $\beta > 0.75$ emit Cherenkov radiation in Counter C*. Antiprotons traversing C* have $\beta < 0.75$, so that they will not emit Cherenkov light in this counter. It was the purpose of C* to distinguish between inelastic events in the target involving the emission of charged particles with $\beta > 0.75$ and all other processes. The particles registering in this counter were predominantly fast charged pions arising from annihilations in the target or in the methyl alcohol of the counter. The efficiency of Counter C* for detecting annihilations was quite high (> 90%) because (a) annihilations are nearly always accompanied by the emission of at least one fast charged pion,[6] and (b) the solid angle subtended by C* at the target was very nearly 4π steradians. S_4 and S_5 are 0.75-in.-thick plastic scintillation counters that were used as "guard" counters to discriminate between charged and neutral particles entering Counter D. Both counters, whose active areas each measured approximately 15 by 15 in., were viewed on two sides by RCA 6810 photomultiplier tubes. Counter D was used to distinguish between antinucleons and all other particles entering it, on the basis of their energy release in D. This counter was constructed in the form of a multilayer sandwich of lead and plastic scintillator viewed by 48 photomultiplier tubes. This type of construction enabled us to obtain a rather thorough

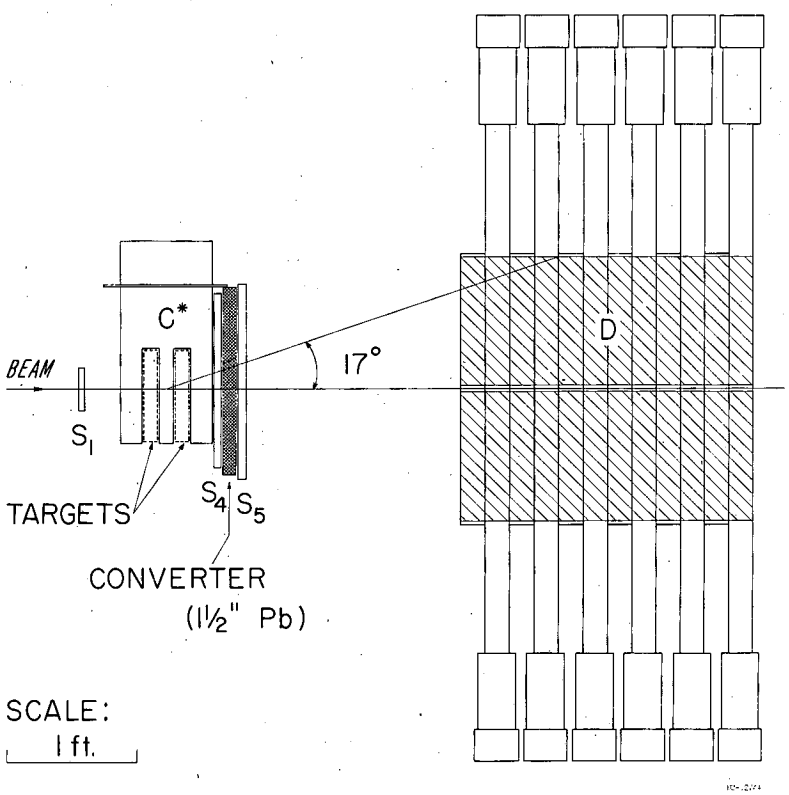

Fig. 2. The system for detection of antineutron production.

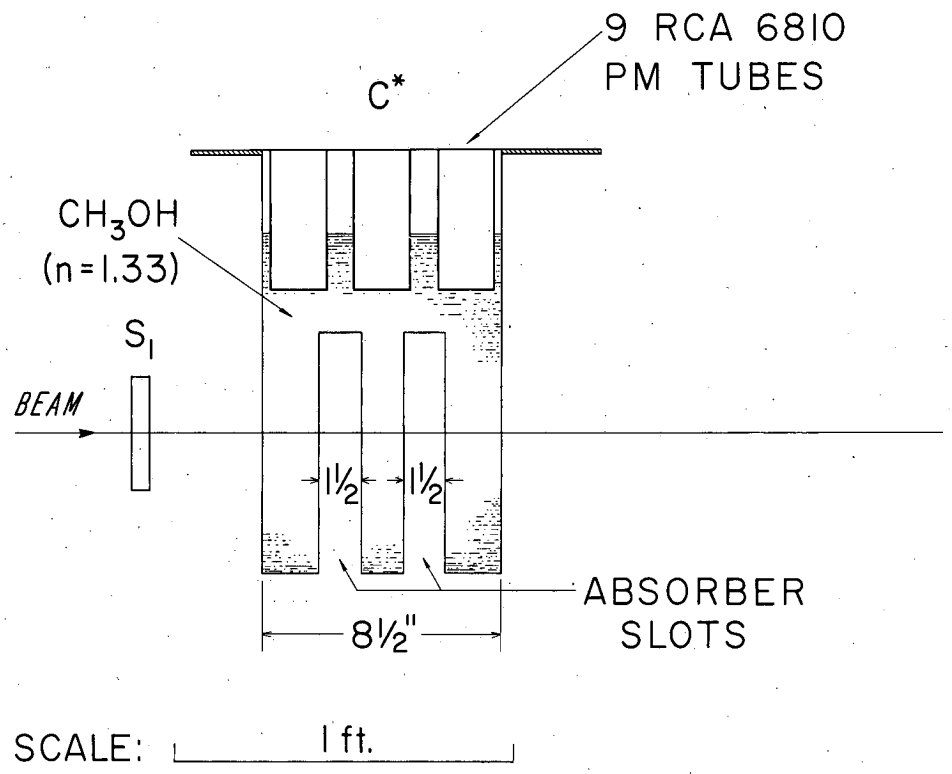

Fig. 3. Schematic view of the Cherenkov counter C* which was used to identify antiproton annihilations in the target.

sampling of the energy released by various particles in this counter. (A detailed description of Counter D is given later, as also are pulse-height distributions observed in this counter for pions and antiprotons of the beam momentum.)

C. Targets

The targets used in antineutron production were polyethylene $(CH_2)_n$, carbon, and lead. The CH_2 and C targets were chosen so that the hydrogen cross section could be obtained by subtraction. The optimum target thickness for production of antineutrons was determined to be that equivalent to one mean free path for attenuation of antiprotons. This would correspond to 40.7 g/cm^2 CH_2, 46.5 g/cm^2 C, and 128 g/cm^2 Pb. However, in order that the target thickness would not become unwieldy and that the average antiproton energy would be approximately the same in the three cases, the target thicknesses given in Table II were chosen. The Cherenkov counter C* was used only with the CH_2 target and contained 11.06 g/cm^2 of methyl alcohol, CH_3OH. The results of this experiment indicate that the charge-exchange cross section per nucleus does not vary appreciably with Z. For this reason we have considered the oxygen atom in the alcohol molecule equivalent to a carbon atom in the production of antineutrons. This assumption leads to the effective CH_2 target thickness and density given in the table. The average antiproton energy $\overline{T}_{\bar{p}}$ in each target is also given.

Table II

Thickness, density, and average antiproton energy for each of the antineutron-production targets.

Target	Thickness (g/cm^2)	Density (g/cm^3)	$\overline{T}_{\bar{p}}$ (Mev)
CH_2	21.4	0.804	455
C	44.6	1.76	434
Pb	86.4	11.35	426

D. Experimental Procedure and Identification of the Charge-Exchange Process

Antiprotons arriving at the target could undergo annihilation, suffer elastic or inelastic scattering, pass through the target and the Cherenkov counter C* without any nuclear interaction, or undergo a charge-exchange process resulting in the formation of a neutron-antineutron pair. Annihilations in the target were in most cases characterized by large pulses in the Cherenkov counter C*. Scattering and pass-through events either did not register in C* or were accompanied by only an occasional small pulse in this counter (the explanation of these small pulses is that methyl alcohol scintillates to a small extent). Pass-through antiprotons or antiprotons scattered into the forward cone defined by Counter D were detected by the guard counters S4 and S5. Charge exchange in the target should not register in the Cherenkov counter C* because no fast charged particles are involved in this reaction. If the antineutron resulting from this process is produced into the cone defined by Counter D and if it does not interact before reaching this counter, we therefore conclude that (a) the antineutron passes through S4 and S5 without counting because it is a neutral particle, and (b) the antineutron annihilates in Counter D, producing a pulse in D corresponding to a 2-Bev energy release in this counter. The formation of an antineutron in the target should thus be characterized by the signal of the arrival of an antiproton in S1 followed by: no pulse in C*, no pulse in the subsequent scintillation counters S4 and S5, and a pulse in D of a size commensurate with that produced by an antinucleon annihilation in this counter (i.e., S1, $\overline{C*}$, $\overline{S4}$, $\overline{S5}$, large pulse in D). The pulse size corresponding to antinucleon annihilation in D was obtained by calibrating this counter with antiprotons.

In the foregoing paragraph we have indicated the various ways in which the antiprotons may interact and we have outlined our method for the detection of the charge-exchange process. We wish to discuss in this section the possible antiproton interactions in more detail and

show how we have "sorted out" the antineutrons from the complex of other particles also passing into Counter D. Antinucleon annihilation with a nucleon of the target nucleus proceeds primarily through the mechanism of pion production followed by nuclear excitation and nucleon emission.[6] Precautions had to be taken to guard against the possibility of confusing any of these annihilation products with antineutrons. Counter C* detected most, but not all, of the antiproton annihilations in the target. Large-angle antiproton scattering could result in the projection of neutrons or protons into Counter D. Charged particles arising from annihilation or antiproton scattering were adequately protected against by the scintillation counters S4 and S5. The most serious problem was to distinguish between antineutrons and all other neutral particles that were also characterized by $\overline{C*}$, $\overline{S4}$, $\overline{S5}$. The response of Counter D is proportional to the amount of energy deposited in it. Thus an analysis of pulse heights in this counter afforded a large measure of protection against these neutral particles. The neutral particles referred to could be neutrons or neutral K mesons (the latter particles arising from annihilations only) that pass through the guard counters unaccompanied by charged particles into Counter D. One of the circumstances under which the Cherenkov counter C* may not register a pulse is when the pions produced in the annihilation are all neutral. The probability of this occurrence is small but it may not be negligible in comparison with antineutron production. The gamma rays resulting from such high-energy neutral pions could simulate antineutrons by giving rise to large pulses in D without being detected by the guard counters. It was the purpose of the 1.5 in. of lead between counters S4 and S5 to convert these gamma rays. In the first run with the CH_2 target, Counter C* was placed in anticoincidence with the others in such a way that an antineutron was defined by a signal from S1 indicating the incidence of an antiproton on the target followed by $\overline{C*}$, $\overline{S4}$, $\overline{S5}$, and a large pulse in D. We found that the information given by C* was superfluous because whenever $\overline{S4}$, $\overline{S5}$ occurred in coincidence with a large pulse in

D there was no pulse in C*. It was then decided to remove the Cherenkov counter C* for the subsequent runs on carbon and lead.

E. Electronics

The signals from counters F1, F2, S1, and C1 were fed into a four-channel coincidence-anticoincidence circuit (resolving time= 4×10^{-9} sec) such that F1, F2, and S1 were in coincidence with one another and in anticoincidence with a pulse from C1. The output signal of this unit (F1, F2, S1, $\overline{C1}$) was then placed in coincidence with a signal from the velocity-selecting Cherenkov counter C2 by means of a second coincidence circuit, AB (resolving time=2×10^{-8} sec). (The lucite radiator in counter C2 was viewed by three photomultiplier tubes.[5] A signal from this counter was defined by a coincidence between signals from any two of the phototubes viewing the lucite radiator).

The pulses from counters C*, S4, S5, and D were displayed on a four-sweep oscilloscope and recorded photographically on Linagraph Pan 35 mm film. The oscilloscope was triggered by a coincidence from the AB circuit (F1, F2, S1, $\overline{C1}$, C2), which, according to the discussion in Section II-A, indicated the arrival of an antiproton in S1. A record of the type of interaction for each antiproton entering the target was obtained in this way. It was also necessary to display the signals from the antiproton-identifying counters, F1, F2, C1, and S1, to supplement the electronic identification discussed above. This was necessary in order to distinguish antiprotons from accidental events occurring because of the large background flux of mesons. The pulses from counters F1, F2, and C1 were displayed on the first sweep of the oscilloscope. Signals from S1 and the Cherenkov counter C* were displayed on the second sweep. Pulses from the guard counters S4 and S5 were shown on the third sweep, and Counter D was displayed on the fourth sweep. The various electronic channels and coincidence units are shown schematically in Fig. 4.

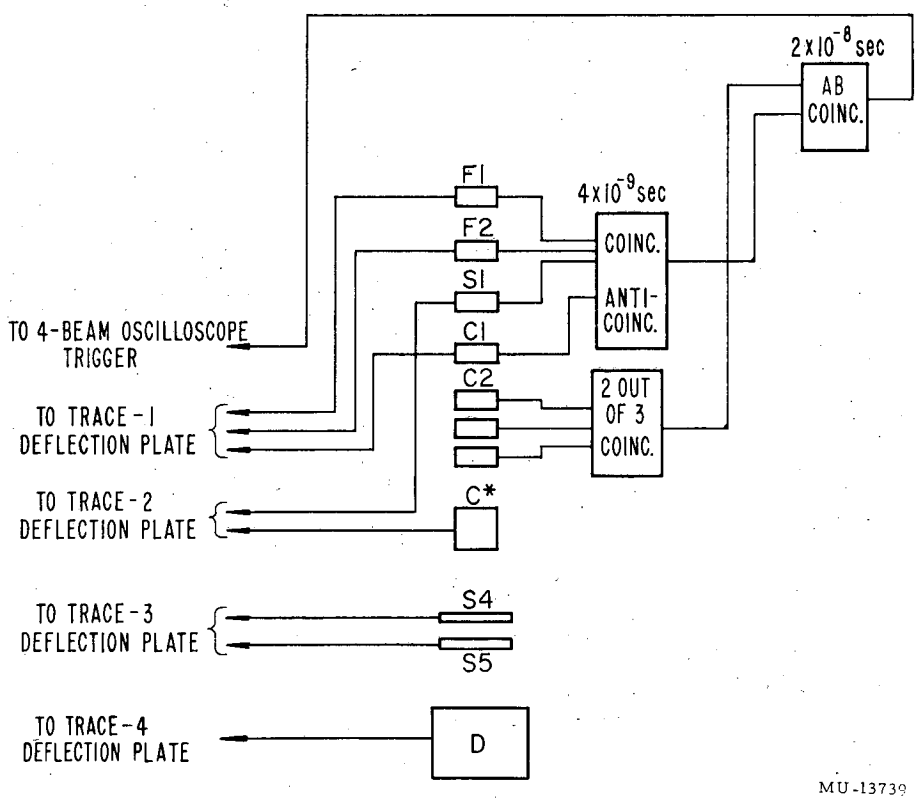

Fig. 4. Schematic diagram of the electronics.

F. Photography and Data Reduction

The 35 mm films were read on Recordak Model C film viewers. Three typical examples of different events for the CH_2 target, as they appeared on the viewer screen, are shown in Fig. 5. Example (a) was typical of antiproton annihilation in the target, which ejected charged particles into Counter D. Case (b) shows an antiproton "pass-through" into D. Example (c) shows an antineutron produced in the target which annihilated in the D counter.

The sweep speed of the oscilloscope was 5×10^{-8} sec/cm, which when magnified on the viewer screen scaled to 10^{-8} sec/cm. The correct separation between the pulses appearing on the four sweeps was required to within $\pm 0.5 \times 10^{-8}$ sec or 0.5 cm on the viewer screen. Traces with spurious pulses occurring within 4×10^{-8} sec (4 cm) before the normal signal or within 2×10^{-8} sec (2 cm) after this signal were rejected in the final analysis although all events were recorded. When the magnetic channel was tuned for a 20% lower mass, and the counter delays were left unchanged, it was found by imposing the above requirements on the traces, that none of the AB electronic coincidences (accidental events due to mesons) could be interpreted as antiprotons. This finding assured us that the antiproton-identifying system was functioning properly.

The pulses occurring on the four sweeps were divided into two groups: (a) signals from F1, F2, C1, and S1, which, properly positioned and free from spurious pulses, completed the identification of an antiproton incident upon the target; (b) signals from C*, S4, S5, and D, which, also satisfying the requirements given above, determined the type of interaction suffered by the antiproton. Observation of pulses in Group (a) were made first and independently of those in Group (b). The identification of an antiproton in Group (a) will be referred to as I_0. The following information was extracted from the pulses in Group (b): pulse heights of C* and D, and a record of the pulses in S4 and S5. The pulse heights were read in mm on the viewer screen.

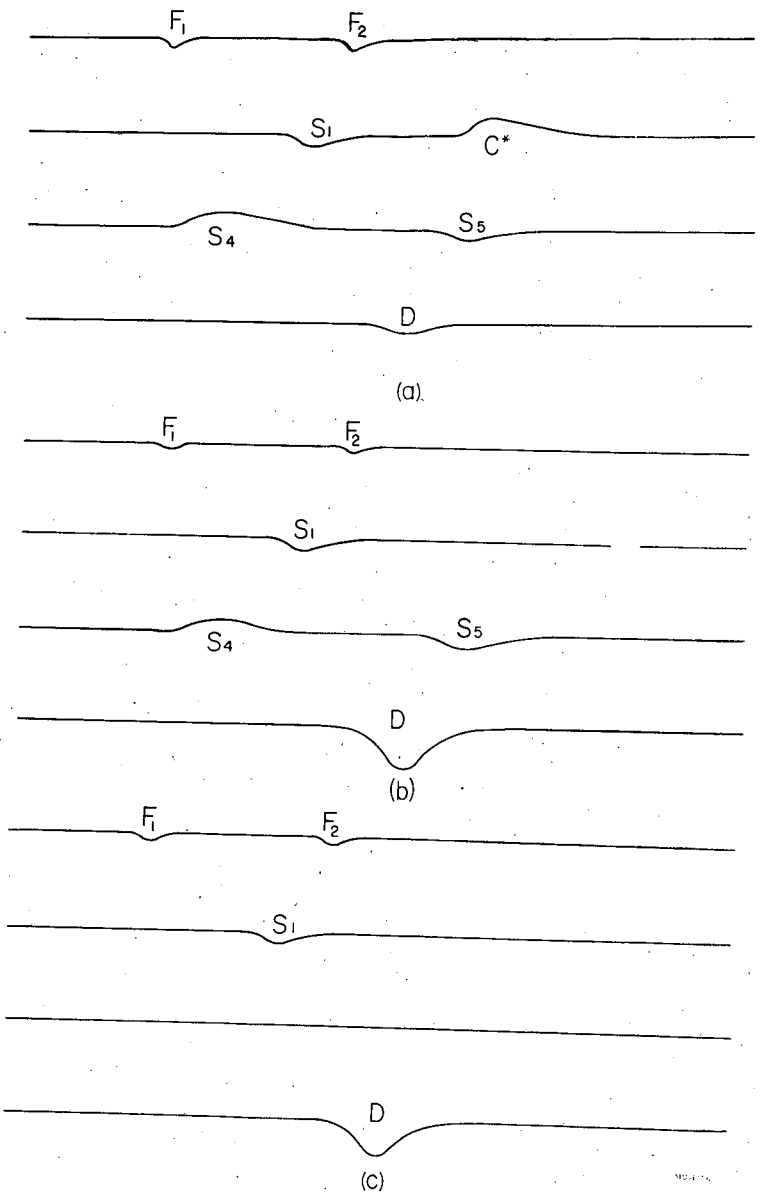

Fig. 5. Oscilloscope record of three antiproton events in the target. The pulses from counters identifying the antiproton F1, F2, C1 were displayed on the top sweep. The signals from the Cherenkov counter C* from the scintillators S1, S4, and S5, and from the counter D were displayed on the lower three sweeps as shown.

(a) An antiproton annihilation in the target sending charged particles into D.

(b) An antiproton pass-through into D.

(c) An antineutron produced in the target and passing into D.

The information obtained upon reading the film was transferred to standard 80-column IBM cards. Analysis of the data was carried out on the IBM 650 magnetic-drum processing machine. The machine rejected all events that did not satisfy the requirements on the traces given at the beginning of this section.

G. Detailed Description of the Antineutron Detector, Counter D

The primary purpose of Counter D was to contain the 2 Bev of energy given up upon antinucleon annihilation in this counter, thereby enabling one to differentiate between antineutrons and other neutral particles also passing into it. In order to make this distinction, this counter was constructed of many layers of thin lead sheets (sufficiently thin so that large amounts of energy would not be absorbed in any one region) and plastic scintillators, so that a good sampling of the energy loss by the various particles incident on the counter could be obtained. Further, we required that the counter present sufficient material to the incident antineutrons so that the annihilation mean free path for these particles in D was small in comparison with the thickness of the counter.

Counter D was constructed of 48 identical cells measuring 24 by 12 by 2 in., each with a sensitive area of 12 by 12 in. A typical cell with the top cover and end plate removed, exposing the laminations of lead and plastic scintillators, is shown in Fig. 6. Each cell contained a 12-by-12-by-2-in. lucite light pipe, six 12-by-12-by-0.25-in. plastic scintillators, and five 12-by-12-in. lead sheets 0.090 in. thick which were sandwiched between alternate layers of the plastic scintillator. The lucite light pipe was made sufficiently large so as to obtain a reasonably uniform response over the active area of the cell. The scintillators were cemented to the lucite with Epon (Shell Chemical Corp. product), and this entire unit was then enclosed in a lighttight steel box. The sides and ends of this container were constructed of 0.25-by-2-in. steel bar. Steel plate 0.125 in. thick was used to cover the top and bottom of each cell. The cells were lined with 0.0015-in. shiny Al foil to reflect as much light into the phototubes as possible.

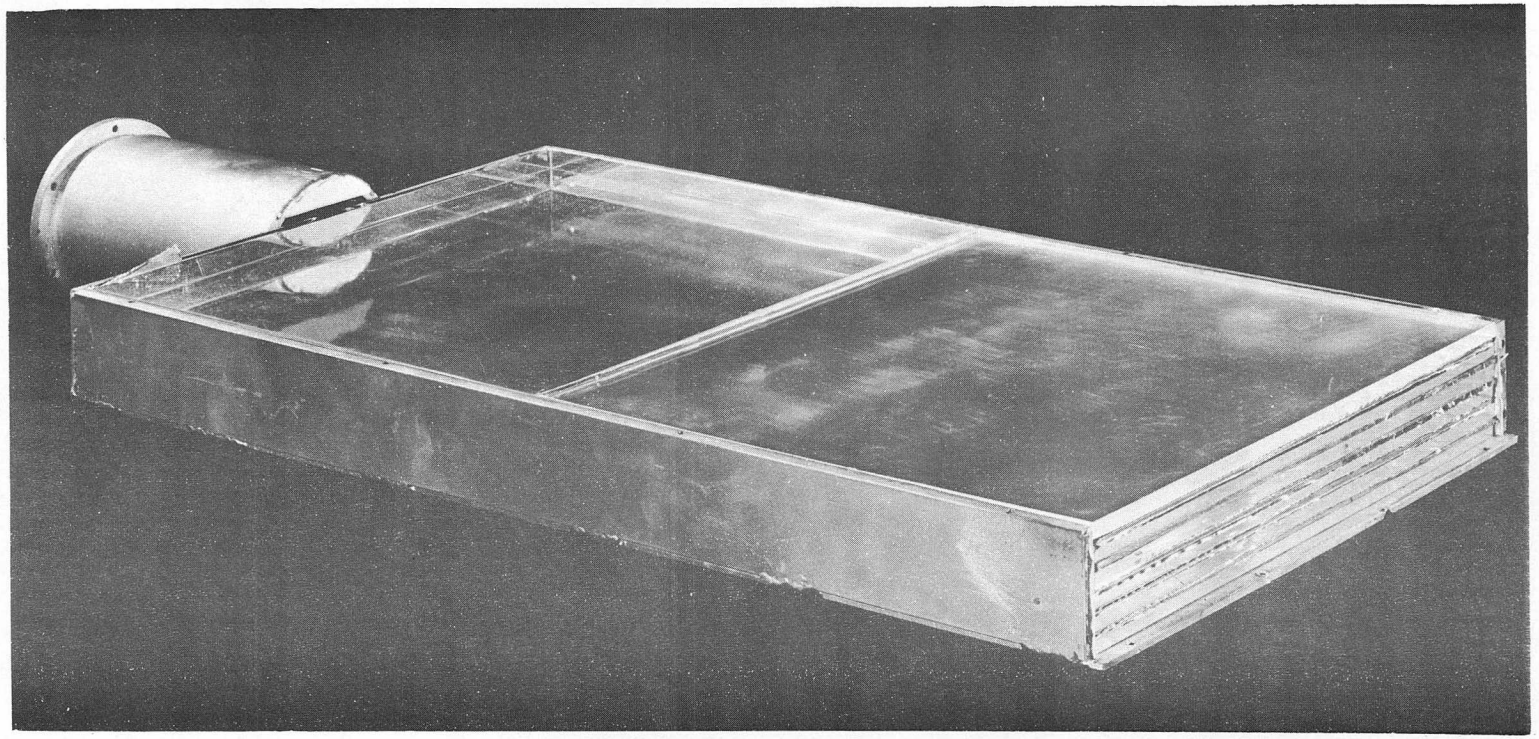

ZN-1604

Fig. 6. A typical cell of Counter D. The steel cover and the end plate have been removed, exposing the laminations of lead and plastic scintillator as well as the lucite light pipe.

Thin Al foils were also inserted between the scintillators and lead sheets for the same purpose. At the end of the cell nearest the lucite light pipe an 8-in.-long iron cylinder with 0.25-in. walls was welded onto the frame to support the tube assembly as well as to afford magnetic shielding to the phototube. Each cell was viewed by a single RCA 6810 photomultiplier tube, which was spring-mounted to the chassis box so that constant pressure was maintained between the tube and the light pipe. Dow-Corning cement was used to complete the light seal between the phototube and the light pipe.

The 48 individual cells were assembled in layers, four cells per layer, so that the entire counter was 12 cells thick along the beam direction. A view of the assembled counter is shown in Fig. 7. The active volume of this counter formed a right parallelepiped measuring approximately 24 by 24 by 27 in. with the long dimension along the beam line. The assembled counter weighed 2.5 tons, and the average density in the sensitive volume was 3.84 g/cm^3. The thickness along the beam direction was 156 g/cm^2 lead, 45.7 g/cm^2 plastic scintillator, and 60 g/cm^2 iron (from the steel covers of the individual cells.) This counter presented approximately three annihilation mean free paths to incident antinucleons and 2.3 mean free paths to high-energy pions that arise from annihilations so that the probability of either particle's escaping from D without making a nuclear interaction was small. Energy carried by gamma rays resulting from neutral pion decay was detected by the electron showers generated in the lead sheets. The lead, scintillator, and iron sheets comprising Counter D were equivalent to 36 radiation lengths. The ionization energy loss of charged particles traversing D was divided in such a way that about 47% was spent in the lead, 25% in the iron, and 28% in the plastic scintillator.

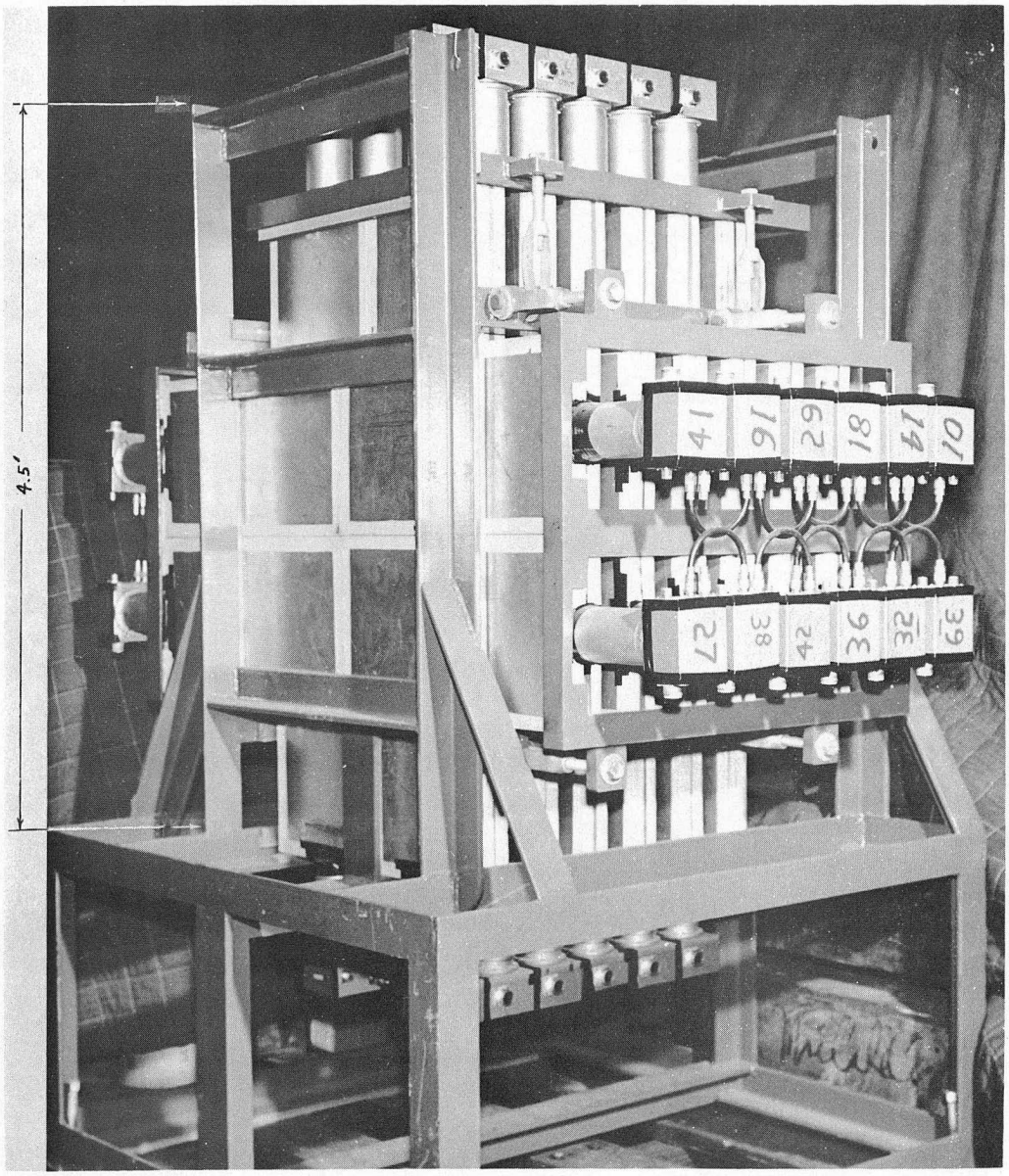

ZN-1747

Fig. 7. The assembled Counter D.

H. Pulse-Height Distributions in Counter D

1. Response of a Single Cell to μ Mesons

In order that Counter D be a reliable energy spectrograph it was necessary that the response of each cell making up this counter be reasonably uniform over the entire active area of the cell. The light arriving at the phototube corresponding to a certain ionization energy loss should not depend on the position at which this energy loss occurred. For checking the response from various portions of the active volume of a cell the following procedure was followed. The 12-by-12-in. active area was marked off into 9 squares measuring 4 by 4 in., as shown in Fig. 8. A counter telescope made up of two small scintillation counters was placed over each of these squares in turn. From coincidences between the counters in the telescope the spectrum was obtained for cosmic-ray μ mesons passing through the active volume defined by each square. In Fig. 9. the resulting μ-meson spectra are plotted. The distributions are numbered 1 through 9 corresponding to the location of the square in which the distribution was obtained. The location of each square is given in Fig. 8. It is observed that the average pulse height does not vary by more than approximately 15% over the entire active area of the cell.

2. π^-, p^+, and $\bar{p}$ Pulse-Height Distributions in Counter D

Range-energy relations indicate that a 1080-Mev/c antiproton is capable of penetrating at most only 16 in. into this counter. Therefore all antiprotons incident upon the central region of D were expected to annihilate. The observed antiproton spectrum for 2000 events is shown in Fig. 10. Most of the "tail" of this curve at small pulse heights (< 7mm) is attributed to antiprotons that annihilated in the lead converter between counters S4 and S5. An additional contribution is due to antiprotons that were scattered by the target and converter into the outer region of D. The dashed histogram in the same figure is the spectrum obtained from negative pions of the same momentum. In Fig. 11 the distribution of pulses produced in D by positive protons of 450 Mev has been plotted.

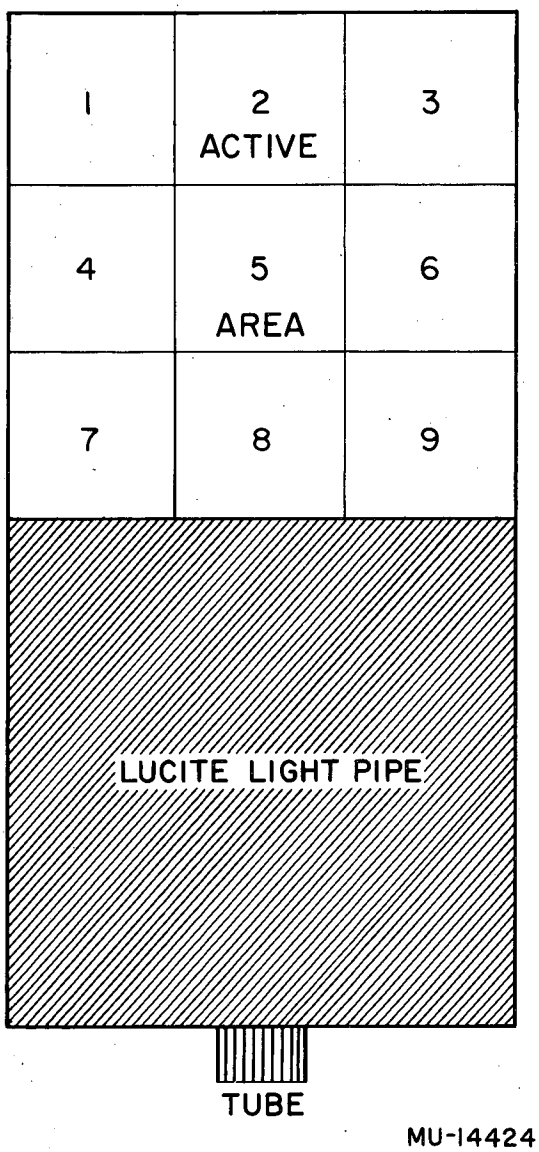

Fig. 8. Top view of a single cell showing the division of the active area into nine 4-by-4-in. squares for the uniformity test.

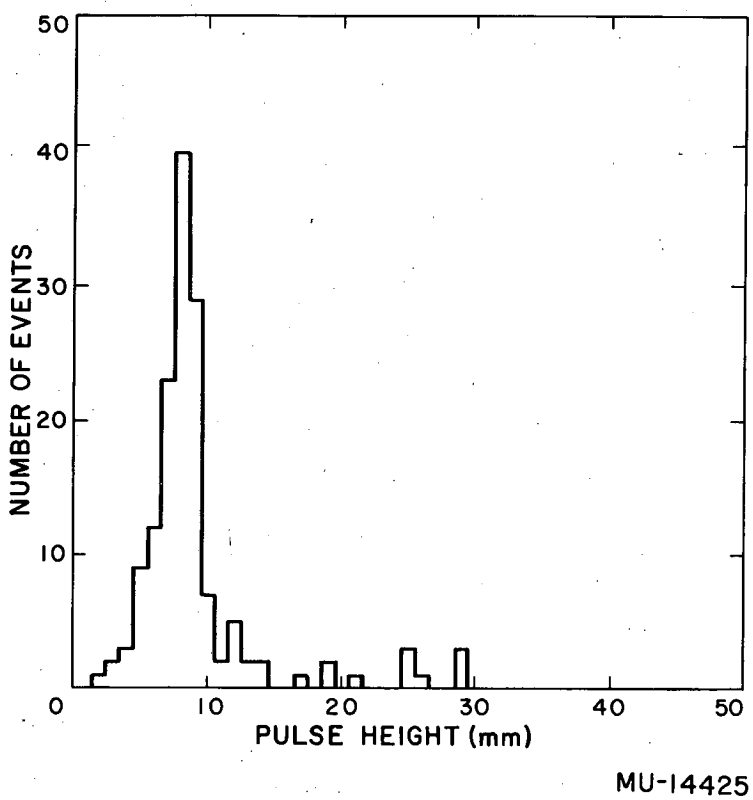

Quadrant I

Fig. 9. Cosmic-ray μ-meson spectra in the nine squares into which the active area of a cell was divided.

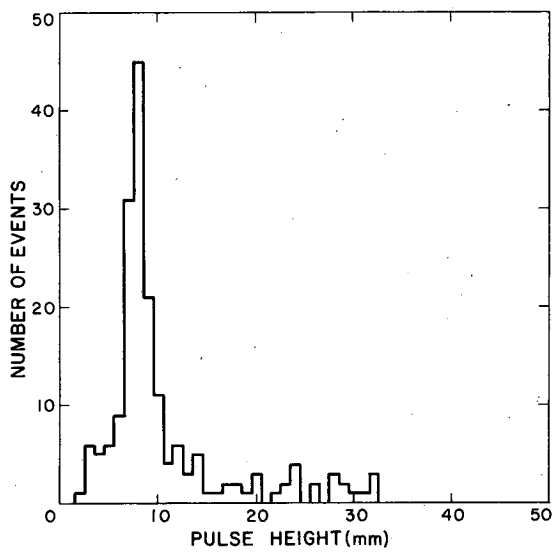

Quadrant II

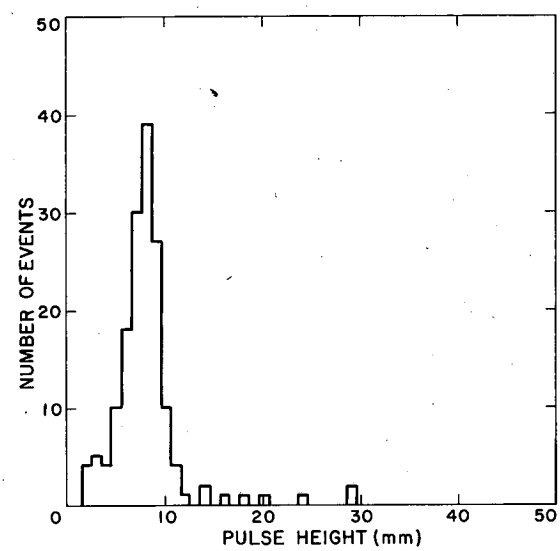

Quadrant III

MU-14426

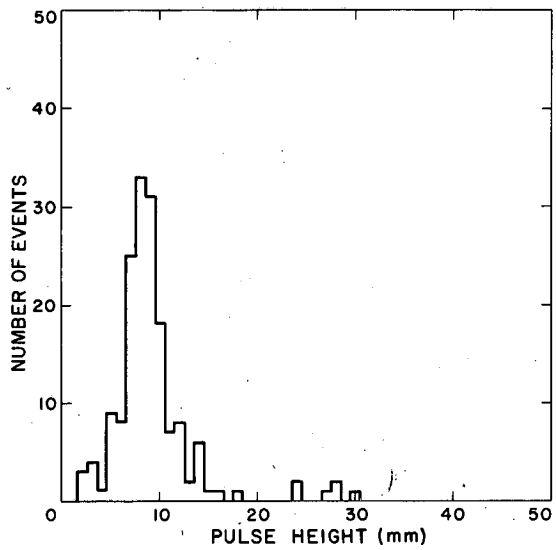

Quadrant IV

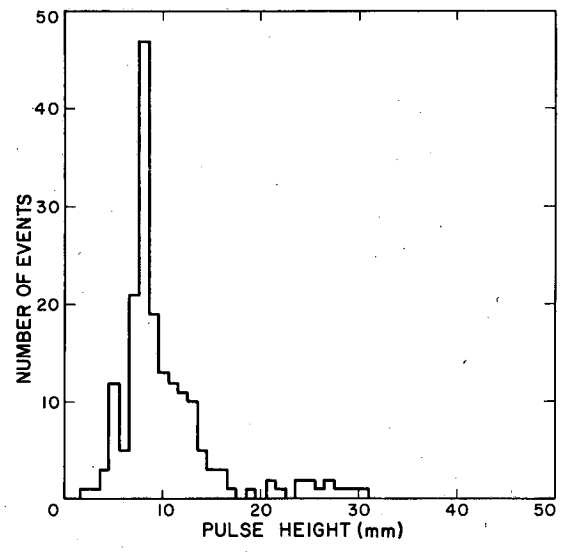

Quadrant V

MU-14427

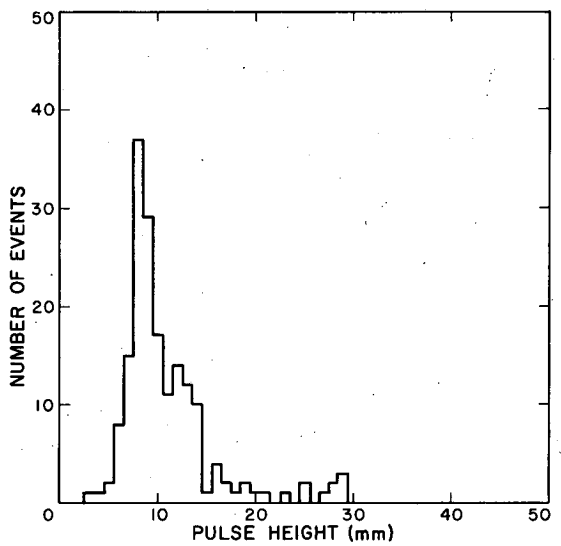

Quadrant VI

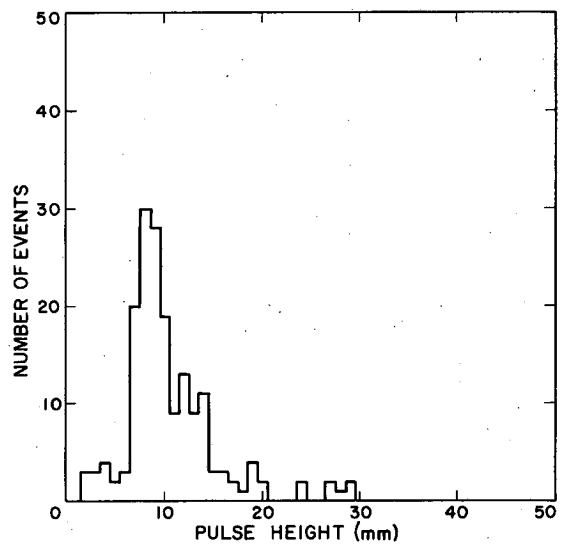

Quadrant VII

MU-14428

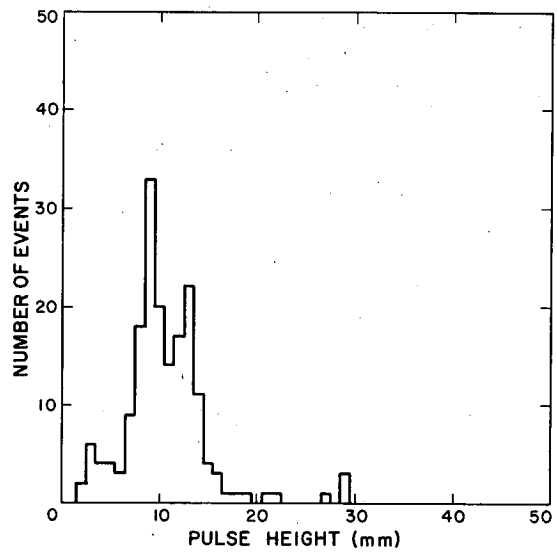

Quadrant VIII

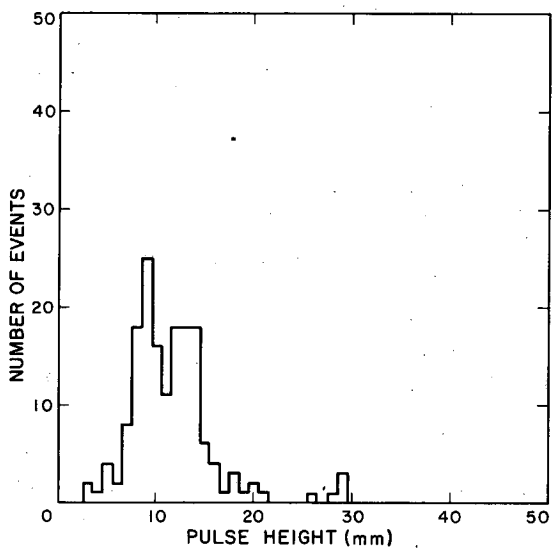

Quadrant IX

MU-14429

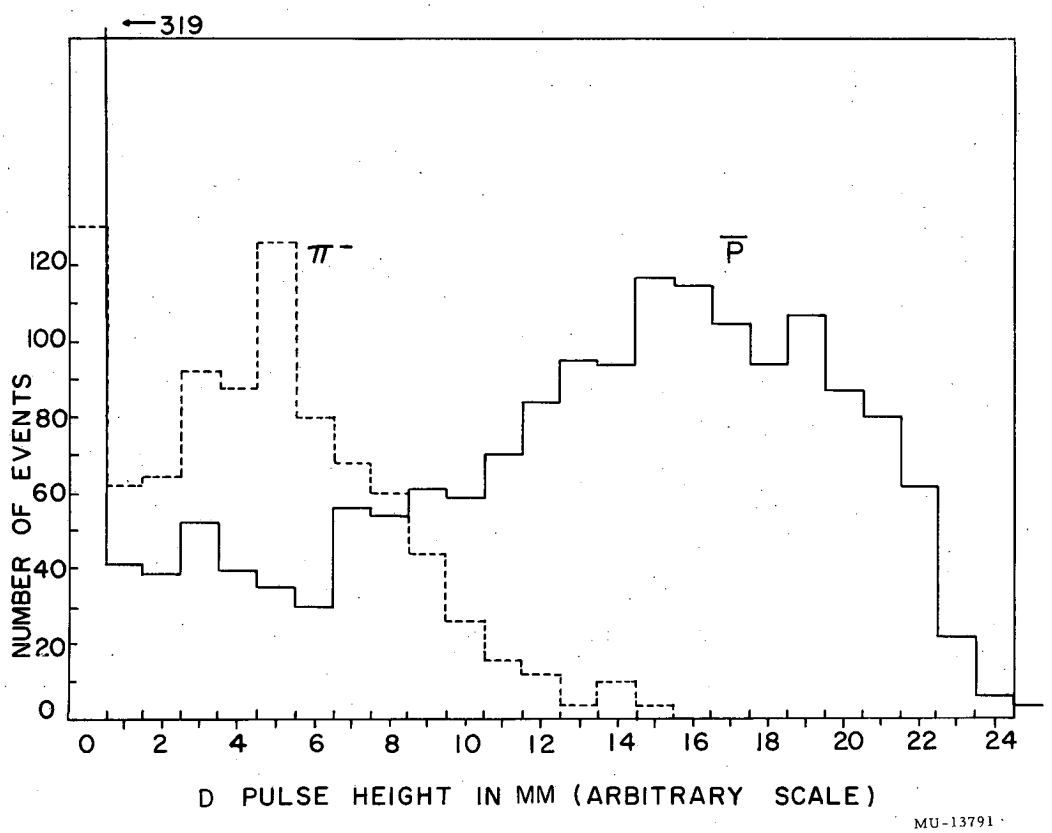

Fig. 10. The solid histogram is the antiproton pulse-height distribution in the D counter for 2000 "pass-through" events in the CH_2 target. The dashed histogram is the π^- spectrum obtained under the same conditions.

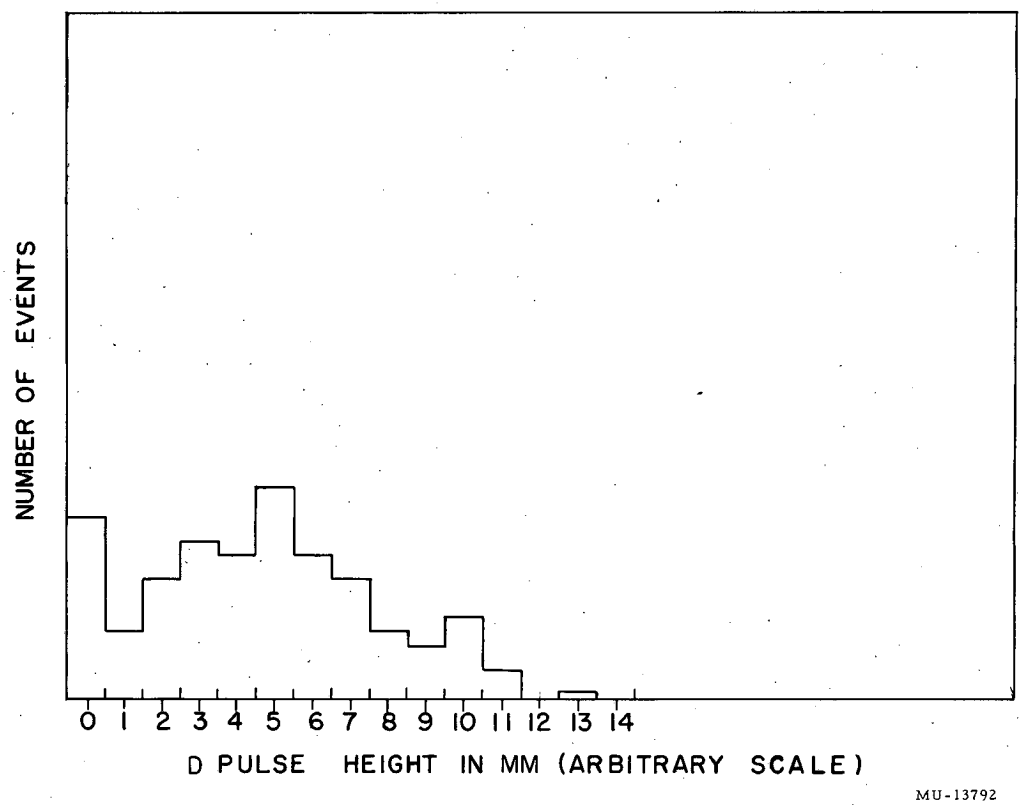

Fig. 11. Pulse-height distribution in D for 450-Mev positive protons incident on this counter.

It might be surprising at first sight that the positive proton and negative pion spectrum in D are so similar, since the latter particle carries much more energy into this counter. However, the chief mechanism by which the two types of particles transfer their energy is quite different. A proton loses energy almost entirely by ionization, whereas the pions lose most of their energy by undergoing an absorption process in nuclei (a pion of the beam momentum loses only 385 Mev by ionization in traversing the full thickness of the D counter, but since the mean free path for pions of this energy is about 12 in. in D it is very probably that they undergo nuclear absorption). In this case a sizable fraction of the energy of the pion goes into fast knock-on nucleons, and some of it is left in the struck nucleus as excitation energy. The resulting fast knock-on neutrons, which carry away about one-half of the knock-on energy, have a mean free path such that there is a good probability of their escaping from the counter without losing any energy. Furthermore, if the struck nucleus is heavy (Pb or Fe) practically all the energy remaining as excitation is given up in the evaporation of neutrons.[7] In conclusion, only a fraction of the energy of the initial negative pion appears in Counter D. Calibration of this counter on the basis of the positive proton spectrum shows that there is an average ionization-energy release in antiproton annihilation of 1350 Mev in the D counter.

III. EXPERIMENTAL RESULTS

A. Antineutron Pulse-Height Distributions in Counter D

Antineutrons that are produced by charge exchange and are projected forward so as to enter D must be characterized by $\overleftarrow{C*}$ (when Counter C* is present), $\overline{S4}$, and $\overline{S5}$. All events that satisfied this condition are recorded in Fig. 12 with the accompanying pulse height in D. In order to confirm the interpretation of these pulses as due to antineutrons we require also that there should be a pulse in D comparable to those observed from antiproton annihilations in this counter. The large pulses appear to be quite consistent with the antiproton spectrum. The grouping at small pulse heights is most probably caused by

(a) inelastic events in the target that have resulted in the entry of neutral particles other than antineutrons into D without giving rise to a pulse in C*, S4, or S5;

(b) antiprotons that have annihilated in the insensitive portion of the D counter, a small part of which was not guarded by the scintillators S4 and S5;

(c) antineutrons produced at an angle with respect to the beam direction such that they were incident near the edge of the active volume of Counter D.

Events of the types (a) and (b) have been observed in other phases of our work to give rise to pulses as large as 5 mm in D. In view of this and also of the requirement that antineutron pulses in D be large, we have classified as antineutrons only those events giving pulses of 7 mm or more in Counter D. With this choice of a cutoff it is seen from the spectra in Fig. 12 that we obtain 13 antineutron events for the CH_2 target, 6 events for the C target, and 1 event for the Pb target.

An exact similarity between the antiproton and antineutron pulse-height distributions in Counter D is not expected. The spectra are dependent upon the spatial distribution of the respective particles

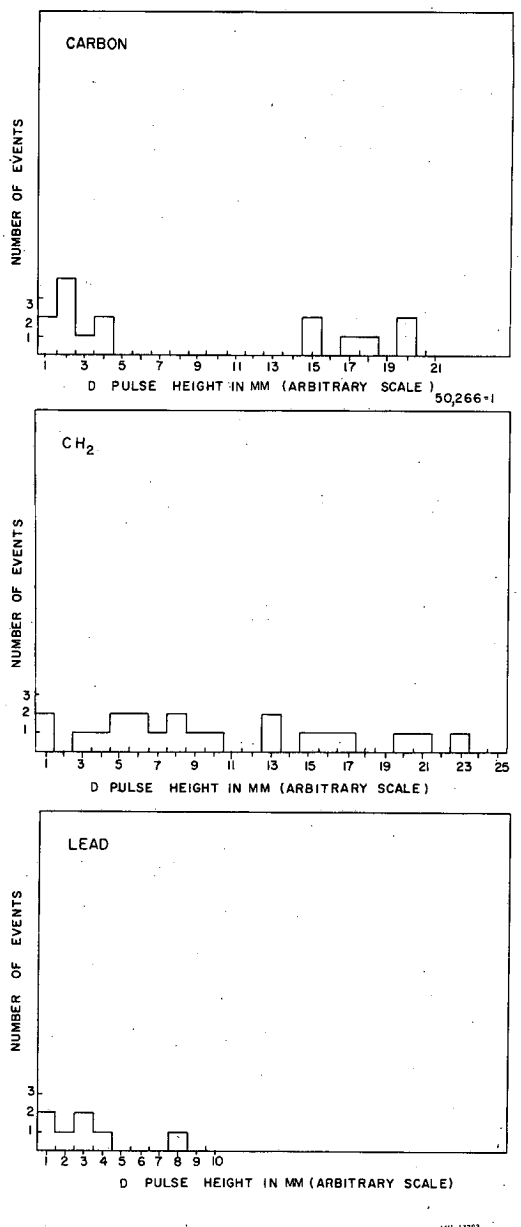

Fig. 12. Pulse-height distribution in Counter D for all events that did not register in S4, S5, and the Cherenkov counter.

over the face of this counter; a distribution that is strongly peaked near 0° differs from one that is uniform in the forward direction in that the latter spectrum is expected to have more events with small D pulse height. This results when annihilation energy escapes detection by the counter, as it would for particles incident and subsequently annihilating near the sides of Counter D. The antineutron distribution is expected to be much broader than the antiproton distribution in the forward direction (in analogy to n-p charge-exchange scattering, $d\sigma/d\Omega$ would be peaked near 0° (lab), but the peak for $(d\sigma/d\Omega)\,\Delta\Omega$ occurs at larger values of θ). For this reason we expect that the antineutron spectrum in D may be flatter than the antiproton distribution in this counter.

B. Sources of Error in Antineutron Detection

1. Requirements of Antineutron Pulse Height in Counter D.

Annihilations occurring in Counter D do not always result in large pulses, as evidenced by the antiproton pulse-height distribution in this counter. On the basis of the antiproton spectra in D we estimate that approximately 10% of the antineutrons entering this counter give rise to pulses less than 7 mm. One possible reason for these small pulses has been given in the preceding section (Case (c)) -- if an antineutron enters near the edge of the active volume of D it may deposit only a small fraction of the annihilation energy in the counter, in which case it causes only a small pulse. The total solid angle subtended by the active volume of Counter D was 0.61 steradian. Antineutrons incident upon this counter in that part of the solid angle near the periphery of D are not expected to give rise to large pulses (as just explained) and are therefore rejected from the acceptable events because they do not satisfy the requirements of pulse height in Counter D. We compensate for the antineutrons that are thus "lost" to us by the following consideration: The effective solid angle within which we detect antineutrons satisfying all the criteria given earlier is taken as having a somewhat smaller value than that actually subtended by Counter D. In determining this "effective" solid angle we imposed the

requirement that all antineutrons produced into this angle should have the opportunity to traverse at least one mean free path for annihilation before escaping from the counter. By assuming an annihilation mean free path in D for the antineutron equal to that for an antiproton we have determined this effective solid angle to be 0.275 steradian, corresponding to a cutoff angle of 17° with respect to the beam direction. This angle is shown in Fig. 3.

2. Possibility of a Count in S4 or S5 Caused by a Charge-Exchange Neutron

The formation of an antineutron in the target passing into Counter D is identified by: I_0, $\overline{C^*}$, $\overline{S4}$, $\overline{S5}$, D ($\gtrsim 7$ mm). The charge-exchange process on free protons or in nuclei is of the form $\bar{p} + p \rightarrow \bar{n} + n$ (see p. 5). We have assumed that the neutron resulting from this process does not undergo any interaction in the target, in C*, or in the 1.5-in. Pb converter that results in a count in C*, S4, or S5. The justification for this assumption is that the antineutrons detected in Counter D come off at small angles (at most 17°) so that the conjugate neutrons acquire only a small kinetic energy, of the order of 20 Mev. If the neutron undergoes an interaction with a proton the latter particle must not only receive sufficient energy to get out of the target into either Scintillator S4 or S5, but it must also be directed toward these counters. The probability, therefore, of the conjugate neutrons giving rise to detectable charged particles is small.

3. Backscattering into Counter D

An additional source of possible error is backscattering from Counter D into S5. Antineutron annihilation in D could result in the backward projection of charged mesons into the guard counters, causing this event to appear as a pass-through antiproton. In setting up the apparatus we attempted to separate the guard counters S4 and S5 from Counter D by as large a distance as practicable without too greatly reducing the effective solid angle for antineutron detection. An estimate of this effect, based on average pion multiplicities observed in

antiproton annihilation in emulsions,[6] indicates that the error introduced by backscattering constitutes a small correction, only of a few percent, which is negligible compared with the statistical error on the number of antineutron events.

C. Antineutron Charge-Exchange Cross Sections

In TableIII the results obtained for each of the targets are summarized. The charge-exchange cross sections were determined from the expression

$$\sigma_c = \frac{I(\bar{n})}{I_0(\bar{p})\, N_{tgt}} \exp\left(N_{tgt}\sigma_{tgt} + N_{sc}\sigma_{sc} + N_{Pb}\sigma_{Pb}\right), \qquad (1)$$

where σ_c = charge-exchange cross section per molecule for production of antineutrons into a solid angle of 0.275 steradian in the forward direction,

$I_0(\bar{p})$ = total number of antiprotons incident on the target,

$I(\bar{n})$ = total number of antineutrons observed in D,

$\exp(N_{tgt}\sigma_{tgt})$, $\exp(N_{sc}\sigma_{sc})$, and $\exp(N_{Pb}\sigma_{Pb})$ are the attenuations in the target, the scintilation counters S4 and S5, and the 1.5-in. Pb converter, respectively. The product of these attenuation factors is between 2.6 and 4 for all targets if we assume the same attenuation cross sections for antineutrons of the energies in this experiment as for 450-Mev antiprotons.

Table III

Summary of experimental results. $I_0(\bar{p})$ is the total number of incident antiprotons, $I(\bar{n})$ is the observed number of antineutrons, and $\overline{T}_{\bar{p}}$ is the average antiproton energy in the target; σ_c is the charge-exchange cross section per molecule for production of an antineutron into a solid angle of 0.275 steradian in the forward direction.

Target	Thickness (g/cm^2)	$I_0(\bar{p})$	$I(\bar{n})$	σ_c (mb)	$\overline{T}_{\bar{p}}$ (Mev)
CH_2	21.4	3647	13	$10.0^{+2.8}_{-2.8}$	463
C	44.6	2738	6	$4.0^{+1.6}_{-1.5}$	438
Pb	86.4	3125	1	$3.8^{+4.2}_{-2.5}$	431

The CH_2 target was used together with the Cherenkov counter C*, which contained 11.07g/cm^2 of methyl alcohol, CH_3OH. We have considered the oxygen atom in the alcohol molecule equivalent to a carbon atom in the production of antineutrons, as mentioned in Section II-C. Because it appears that the charge-exchange cross section does not vary rapidly with Z, this step is justified and leads to the effective CH_2 target thickness given in Table III. The indications that the charge-exchange cross sections for different nuclei are approximately constant is also predicted by optical-model calculations, which are discussed in Section IV. Total antiproton cross sections for cutoff angles of 17° in lead and oxygen, as well as a value for the total $\bar{p}$-n cross section, were obtained from experiments described in References 8 and 9. The antiproton cross section for carbon was determined from the measured value on oxygen by use of the relationship $\sigma_C = \sigma_O \ (A_C/A_O)^{2/3}$, where A_C and A_O are the mass numbers of carbon and oxygen respectively. Using these cross sections and the given thickness of the targets, the scintillators S4 and S5, and the lead converter, we obtain the following values for the attenuation factor appearing in the expression for σ_c:

CH_2 target, $\exp(\Sigma N\sigma) = 2.6 \pm 0.10$;

C target, $\exp(\Sigma N\sigma) = 4.01 \pm 0.16$;

Pd target, $\exp(\Sigma N\sigma) = 3.01 \pm 0.21$.

A value for $(\bar{p} + p \rightarrow \bar{n} + n)$ can be obtained from the CH_2 and C data by subtraction. We find

$$\sigma \ (\bar{p} + p \rightarrow \bar{n} + n) = (3.0 \pm 1.6) \times 10^{-27} \text{ cm}^2$$

for antineutron production by protons into a solid angle of 0.275 steradian in the forward direction. This value corresponds to a differential cross section of $(10.9 \pm 5.8) \times 10^{-27}$ cm^2/steradian averaged over a cone of half-angle 17° in the forward direction.

The errors accompanying the various cross sections are standard deviations due to counting statistics only. They were determined

from the expression $\Delta \sigma_c = \Delta I(\bar{n})\sigma_c / I(\bar{n})$ where, because of the small number of events involved, $\Delta I(\bar{n})$ is obtained from a Poisson distribution. The error associated with the exponential in σ_c due to the uncertainty in the antiproton cross sections is negligible compared with the statistical error on $I(\bar{n})$.

The charge-exchange cross sections may be obtained without reference to the antiproton attenuation cross sections. If the exponential is combined with $I_0(\bar{p})$ in Eq. (1), we obtain

$$\sigma_c = I(\bar{n}) / I(\bar{p}) N_{tgt} , \qquad (2)$$

where $I(\bar{p})$ is the number of antiprotons passing through the target C*, S4, S5, and the 1.5-in. lead converter into Counter D. This follows from Eq. (1) and the relationship

$$I(\bar{p}) = I_0(\bar{p}) \exp-(N_{tgt}\sigma_{tgt} + N_{sc}\sigma_{sc} + N_{Pb}\sigma_{Pb})$$

$$= (\text{no. of incident antiprotons}) \times (\text{total attenuation factor for angles } > 17^{\circ}) .$$

The value of $I(\bar{p})$ is obtained from the D spectrum by using the same criteria in regard to D pulse height as were used to determine $I(\bar{n})$. Namely, $I(\bar{p})$ is the total number of events satisfying: I_0 (the identification of an antiproton incident upon the target), a pulse in S4 and S5, and a pulse in D greater than or equal to 7 mm. A study of C* pulse height versus D pulse height indicates that a small correction (about 8%) must be made to $I(\bar{p})$ obtained in this way to take into account annihilations in the target and lead converter that are accompanied by large pulses in D. These relatively rare events are due to annihilations in which a sizable fraction of the annihilation energy is sent forward into Counter D, causing a large pulse in this counter. Table IV lists the quantities $I(\bar{p})$, $I^*(\bar{p})$ (the corrected value of $I(\bar{p})$ used in Relation (2)), and the value for the charge-exchange cross section, σ_c, obtained by this method. It is observed that the two methods for obtaining the charge-exchange cross section are in agreement.

Table IV

Values for σ_c per molecule for the production of an antineutron into a solid angle of 0.275 steradian in the forward direction calculated from Relation 2. $I(\bar{p})$ is the number of antiprotons passing into Counter D assuming that all events I_0, S4, S5, D $\gtrsim$ 7 mm are pass-through antiprotons. $I^*(\bar{p})$ is a corrected value for $I(\bar{p})$ which takes into account annihilations in the target and lead converter that are accompanied by large pulses in D and are included in $I(\bar{p})$.

Target	$I(\bar{p})$	$I^*(\bar{p})$	σ_c (mb)
CH_2	1517	1394	$10.2 \begin{cases} +2.8 \\ -2.8 \end{cases}$
C	752	691	$3.9 \begin{cases} +1.6 \\ -1.5 \end{cases}$
Pb	1144	1051	$3.8 \begin{cases} +4.2 \\ -2.5 \end{cases}$

The charge-exchange cross section for carbon given above should be compared with the estimate of 8×10^{-27} cm^2 given by Cork, Lambertson, Piccioni, and Wenzel[2] for charge exchange into a comparable solid angle.

IV. DISCUSSION

The experimental results show that the charge-exchange cross sections for lead, carbon, and hydrogen are the same within statistical limits. This indicates that the effective charge-exchange cross section per proton of the target nucleus decreases rapidly with increasing Z. Much of this decreases can be attributed to the large nucleon-antinucleon annihilation cross section. This large cross section has two effects: first, it prevents antiprotons from penetrating into the nucleus and thus leaves only the hemispherical surface of the nucleus, which the beam strikes first, effective in producing antineutrons. Secondly, most of the antineutrons that are produced in the forward direction at this surface are swallowed up before they can escape from the nucleus. We may therefore expect that observable antineutrons are produced only when the incident antiprotons make a grazing collision with the nucleus. This can be understood if we recall that near the nuclear periphery the density of nucleons is probably much less than it is in the central region. Furthermore, in grazing collisions the geometrical path length of the antinucleon in nuclear matter is small. Emulsion studies indicate that antiproton annihilations actually do tend to occur near the nuclear surface before the incident antiprotons can enter the region of high nucleon density.[6] Hence, it would seem reasonable that to incident antinucleons the nucleus appears as a black absorbing disk surrounded by a grey region of partial transparency. In this model observable antineutrons would be produced only in the grey region, the size and greyness of which is governed by the shape of the nucleon density distribution. In the following section we investigate the effect of various density distributions, using an optical model. Neutron-antiproton collisions are less likely to give rise to antineutrons than proton-antiproton collisions because the emission of an antineutron in a $\bar{p}$-n collision requires the formation of at least one negative pion, which is energetically unfavorable and competes poorly with the process $\bar{p} + p \rightarrow \bar{n} + n$, as indicated in Appendix I. This circumstance is an

additional reason for further depression of charge exchange in heavy nuclei, because the ratio N/Z is higher for these nuclei than it is for light nuclei.

A. Optical-Model Predictions for the Antineutron-Production Cross Sections on Complex Nuclei

To examine the ideas expressed above in more detail, we have calculated values for the charge-exchange cross section on various nuclei using an optical model and compared the results of these calculations with the experimental values on carbon and lead. This model requires knowledge of the $\bar{p}p$, $\bar{p}n$, $\bar{n}p$ and $\bar{n}n$ attenuation cross sections (we assume in what follows that we have $\sigma_{\bar{p}n} = \sigma_{\bar{n}p}$ and $\sigma_{\bar{p}p} = \sigma_{\bar{n}n}$), the $\bar{p}p$ charge-exchange cross section, and the density distribution of nucleons in the nucleus. The formula we obtain for the charge-exchange cross section per nucleus for production into a cone of half angle 17° with respect to the beam direction is given by

$$\sigma_c(A) = 4\pi(Z/A)\,\overline{\sigma_c(H)} \int_0^\infty b\,db \exp\left(-2\sigma^t \int_0^\infty \rho(r)ds\right) \int_0^\infty \rho(r)ds, \qquad (3)$$

where Z = nuclear charge,

A = mass number of nucleus under consideration,

$\overline{\sigma_c(H)}$ = $(\bar{p}$-$p)$ charge-exchange cross section for production into a cone of half angle 17° with respect to the beam direction,

σ^t = total nucleon-antinucleon cross section for angles $> 17^\circ$ (the selection of this cutoff for σ^t is somewhat arbitrary),

$\rho(r)$ = density distribution of nucleons in nucleus,

s = distance measured from the center of the nucleus along the beam direction,

b = distance measured from the center of the nucleus perpendicular to the beam direction.

Equation (3) has been derived on the assumption of a well-defined trajectory for the incident antiprotons and a spherically symmetric distribution of nucleons given by $\rho(r)$. There are two necessary considerations for the validity of this expression:[10] First, both the

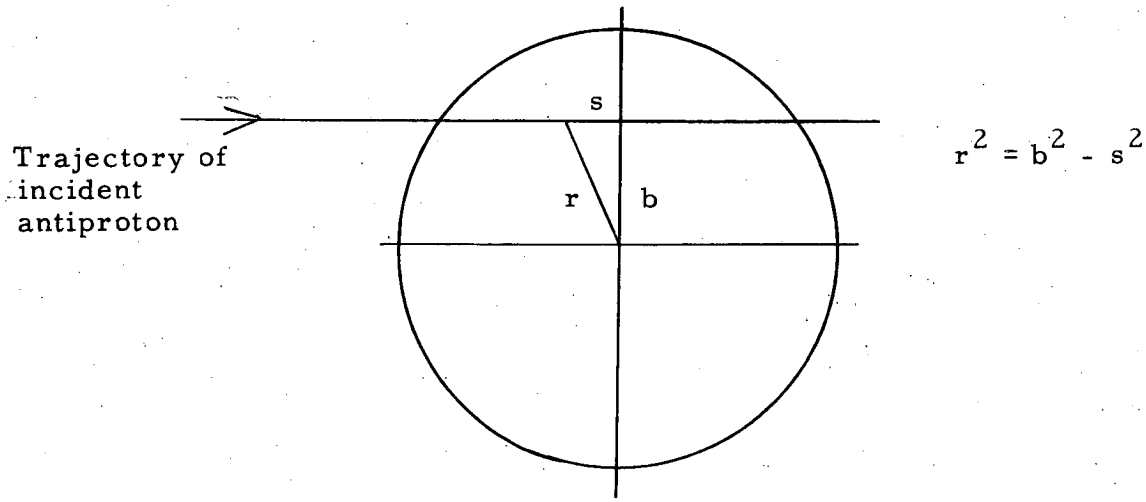

Fig. 13. Representation of optical model, showing variables s, b, and r appearing in Eq. (3).

DeBroglie wavelength of the antinucleon and the nucleon-antinucleon interactions radius must be smaller than the spacing between nucleons; and second, the mass number of the nucleus must not be too small. The spacing between nucleons depends on the density distribution $\rho(r)$. The nucleon-antinucleon interaction radius determined from the expression

$$r_o = \sqrt{\sigma^t/\pi} = 1.8 \times 10^{-13} \text{ cm},$$

where σ^t is the antinucleon-nucleon attenuation cross section, is of the same order of magnitude as the spacing between nucleons in the central region of the nucleus for the most commonly used density distributions. Thus, it appears that the necessary condition on the smallness of the range of the force is violated. However, as discussed previously, we expect greatest production of observable antineutrons to occur at the nuclear surface, where the density is small. In this region of reduced density the requirement on the range is more nearly satisfied.

The $\overline{p}$-n and the $\overline{p}$-p attenuation cross sections at 450 Mev are the same within statistical limits.[9] We have assumed, in the derivation of

Eq. (3), that only $\bar{p}$-p collisions give rise to antineutrons. Because of the equality between the $\bar{p}$-p and $\bar{p}$-n cross sections (which are assumed equal to the $\bar{n}$-p and $\bar{n}$-n respectively) only one attenuation cross section appears in Eq. (3), the value of which we take as 104 mb.[9] The value for the $\bar{p}$-p charge-exchange cross section, $\overline{\sigma_c(H)}$, has been obtained from the CH_2 and C data by subtraction as discussed in Section III C, where it is given as $3.0 \pm 1.6 \times 10^{-27}$ cm^2.

The effect of the following nuclear density distributions in Eq. (3) has been investigated. These distributions are discussed in Hofstader's paper on electron scattering,[11] and the parameters appearing in these expressions were chosen so as to give the best fits to the density of charge in the nucleus as seen by the electrons. We assume that the nucleon distribution is the same as the charge distribution.

(a) Uniform or rectangular distribution:

$$\rho(r) = \rho_1, \qquad 0 < r < R,$$
$$\rho(r) = 0, \qquad r \geq R,$$

where we take $R = 1.25A^{1/3} \times 10^{-13}$ cm.

(b) Trapezoidal distribution:

$$\rho(r) = \rho_2, \qquad 0 < r \leq c - Z_2,$$
$$\rho(r) = \rho_2(c+Z_2-r)/2Z_2, \qquad c - Z_2 < r < c - Z_2,$$
$$\rho(r) = 0, \qquad r \geq c - Z_2,$$

where $2Z_2$ is the radial distance in which the density falls from its maximum value (ρ_2) to zero. The parameter c, referred to as the radius parameter, is the distance at which the density has fallen to one-half its maximum value. Following Hofstader we choose

$$c = 1.08A^{1/3} \times 10^{-13} \text{ cm},$$

$$Z_2 = 1.5 \times 10^{-13} \text{ cm}.$$

(c) Uniform Fermi distribution:

$$\rho(r) = \rho_3/\left[\exp\left(\frac{r-c}{Z_3}\right) + 1\right],$$

where c is the radius parameter and taken as $1.08A^{1/3} \times 10^{-13}$ cm.[11]

The quantity Z_3 is related to the skin thickness t (radial distance in which the density falls from 90% to 10% of its maximum value) by the relation $Z_3 = t/4.40$. The thickness t, which the electron-scattering experiments indicate is approximately a constant for all nuclei with $Z \geq 6$, is taken as 2.4×10^{-13} cm for each of the nuclei to be studied.

The constants ρ_1, ρ_2, ρ_3 appearing in each of the expressions for the density functions are evaluated from the condition $\int \rho(r)\, d^3r = A$, where A is the mass number of the nucleus. A plot of the trapezoidal and uniform Fermi nucleon densities for lead is given in Fig. 14, demonstrating the differences between these distributions. The various density distributions have been inserted in Eq. (3), and charge-exchange cross sections for C, Fe, Ag, and Pb have been obtained by numerical integration of this expression on the IBM 650 computer. These cross sections are listed in Table V along with the experimental values for C and Pb.

The cross sections obtained from Eq. (3) for the uniform density are too small by a factor that is on the order of 10. The values obtained by use of the Fermi density are consistent with the experimental cross sections. These results confirm our eariler prediction that the major production of observable antineutrons takes place at the "tail" of the density distribution, where the nucleon density is low. The reason for this appears to be that the spacing between nucleons is such that only in this region does an antiproton or an antineutron have a chance of surviving without undergoing annihilation.

Up to this point we have neglected the effect of the finite range of interaction between the antinucleon and nucleon on the density distribution. The trapezoidal and uniform Fermi densities introduced previously are best fits to the density of charge in the nucleus as determined by the electron-scattering experiments.[11] In the ensuing calculations we assumed that the nuclear density as seen by the antinucleon is the same as that seen by the electron. This is not strictly correct and can be seen from the following argument. The electron-scattering experiments ascribe an electromagnetic interaction radius to the proton equal to approximately 0.77×10^{-13} cm,[11] whereas the

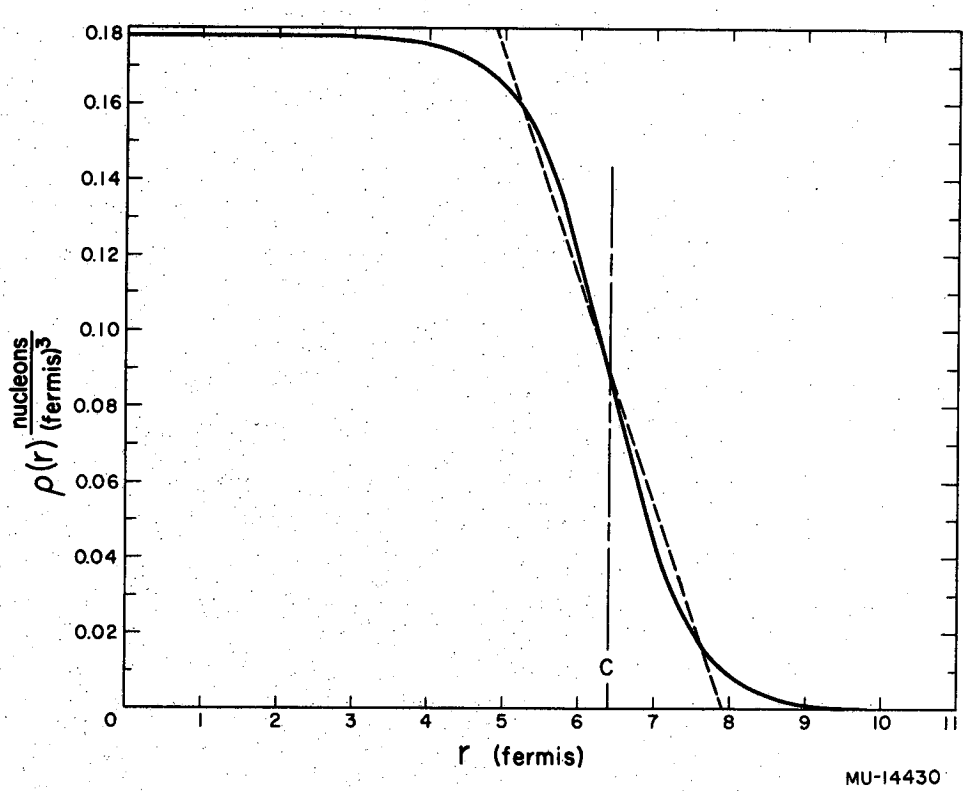

Fig. 14. Plot of the trapezoidal and uniform Fermi nucleon densities for Pb. Solid curve: uniform Fermi distribution. Dashed curve: trapezoidal distribution.

Table V

Optical-model predictions of charge-exchange cross sections for various elements. All cross sections are for production into a cone of half angle 17^{o} in the forward direction.

Element	σ_c				
	Rectangular nucleon distribution (mb)	Trapezoidal distribution (mb)	Uniform Fermi distribution (mb)	Modified Fermi distribution (mb)	Experimental values (mb)
Carbon	0.28	1.3	2.2	3.4	$4.0^{+1.6}_{-1.5}$
Iron	0.26	1.4	2.9	4.2	-------
Silver	0.25	1.5	3.2	4.5	-------
Lead	0.22	1.5	3.4	4.4	$3.8^{+4.2}_{-2.5}$

proton-antiproton system is governed by an interaction radius on the order of 1.8×10^{-13} cm, as indicated earlier. The effect of this larger radius of interaction is that the antinucleon "sees" a density distribution that is more smeared out than that seen by the electron.

Williams includes the effect of the range by folding the density distribution for the electric charge into a resolution function for the finite range of influence of the nucleon,[12] forming the integral

$$\rho'(r) = \int F(|\vec{r} - \vec{r}'|)\, \rho(r')\, d^3r' . \qquad (4)$$

Here $F(|\vec{r} - \vec{r}'|)$ is the resolution function designating the space dependence of the antinucleon-nucleon interaction and $\rho'(r)$ is the modified density distribution seen by the antinucleon. We note that when $F(|\vec{r} - \vec{r}'|)$ assumes the form of a delta function the integral above reduces to $\rho(r)$, so that the effect of the finite range vanishes as it should. For the function $F(|\vec{r} - \vec{r}'|)$ we have chosen a square well of range r_0 equal to the nucleon-antinucleon interaction radius, 1.8×10^{-13} cm. The density function $\rho(r')$ that we have used in Eq. (4) is the uniform Fermi distribution discussed earlier. Numerical integration of this expression was performed on the IBM 650 computer to obtain the modified Fermi densities for the four elements C, Fe, Ag, and Pb. A plot of the uniform Fermi and the modified Fermi distributions is given in Fig. 15, in which the smearing effect of the finite range is quite noticeable. The modified density functions for the four elements were inserted into Eq. (3) and the solution was obtained on the IBM 650 computer. The resulting charge-exchange cross sections are listed in the fourth column of Table V. We note that the cross sections obtained by use of the modified Fermi distribution are somewhat larger than those obtained from the uniform Fermi density. This is attributable to the smearing effect of the finite range, which effectively increases the amount of tail in the nucleon distribution.

Figure 16 is a plot of the charge-exchange cross section as a function of nuclear charge Z for each of the nuclear densities investigated. Because of the poor counting statistics our results are consistent with

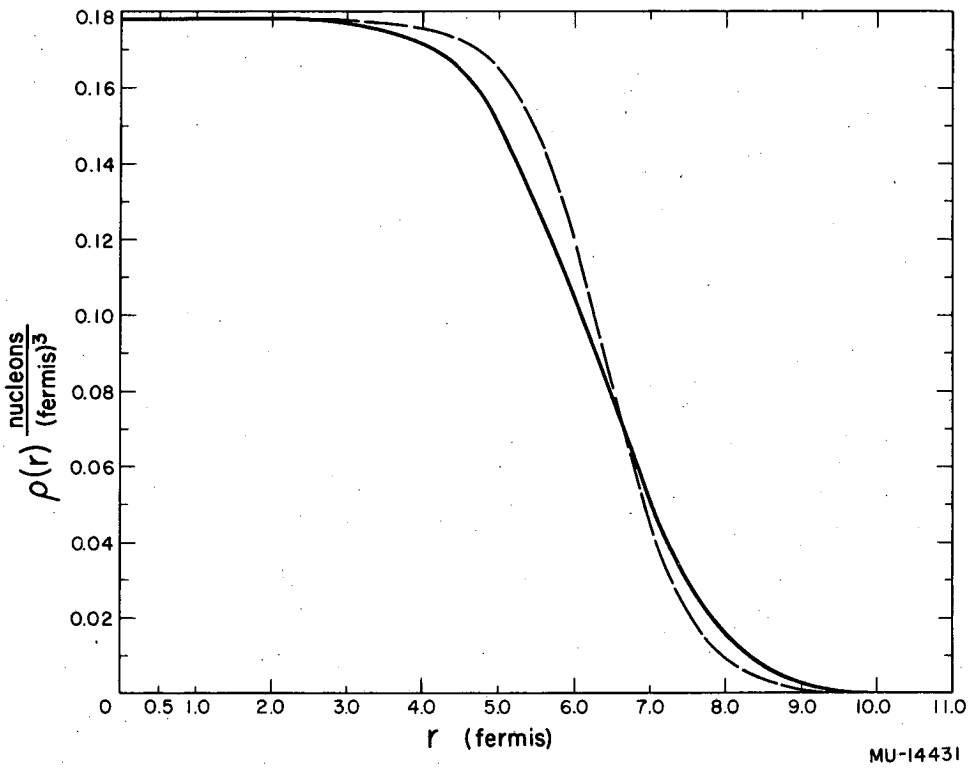

Fig. 15. Plot of the uniform Fermi and modified Fermi nucleon distributions. Dashed curve: uniform Fermi distribution. Solid curve: modified Fermi distribution.

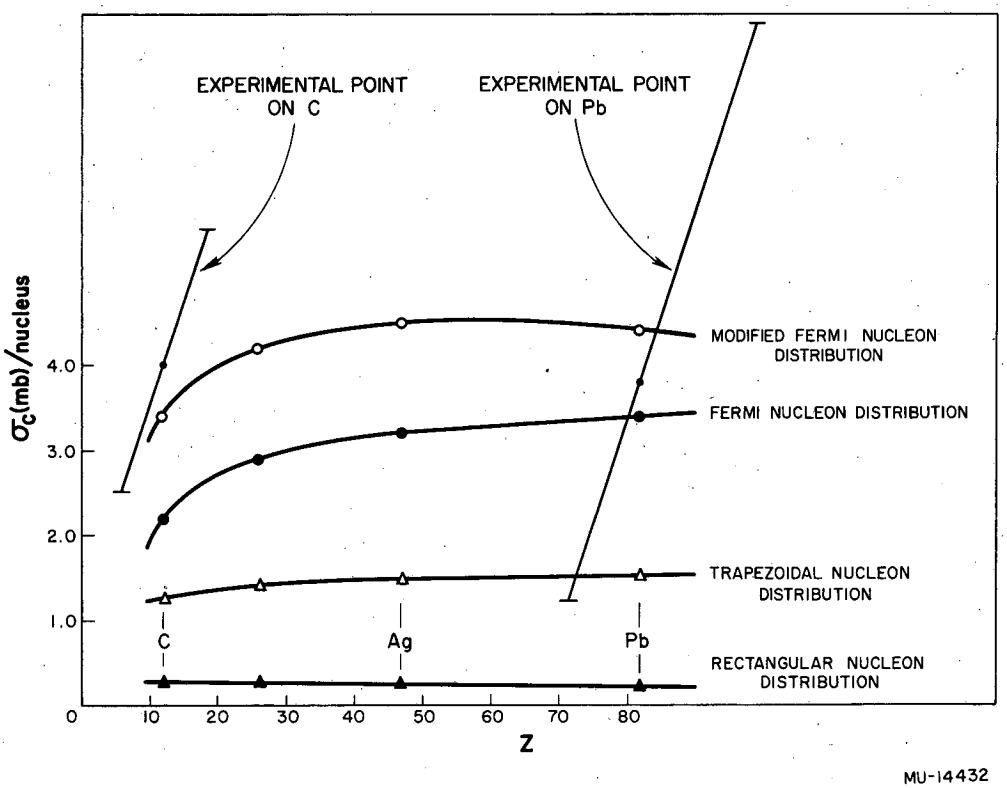

Fig. 16. Plot of the charge exchange cross section per nucleus as a function of Z for each of the four nucleon density distributions investigated.

all the density distributions with the exception, perhaps, of the uniform distribution. Finally, it should be noted that the charge-exchange cross sections for heavy nuclei may be somewhat smaller than the values predicted on the basis of the optical model above. There are reasons to believe that there are more neutrons than protons near the surfaces of these nuclei.[13, 14] If there are more, the exchange process would be considerably depressed in heavy nuclei because fewer protons would be available near the nuclear surface to enter into this reaction.

B. Comparison With n-p Charge Exchange Scattering

If we assume that the angular distribution of the $\bar{p}$-p charge-exchange cross section is the same as that for the n-p exchange process, we find that approximately 40% of the charge-exchange antineutrons should be produced into the solid angle defined by Counter D. This comparison also leads to an estimate of the $\bar{p} + p \rightarrow \bar{n} + n$ differential cross section at 0° (lab) of 38 ± 20 mb, which is to be compared with a value of 54 mb at the same lab angle for the p-n charge-exchange cross section at 400 Mev.[18]

C. Consequences of Charge Independence Applied to the Antinucleon-Nucleon System

Charge independence requires that the following inequality be satisifed:

$$\frac{d\sigma}{d\Omega}(0^\circ)_{\bar{p}p \rightarrow \bar{n}n} \geq (k/4\pi)^2 \left[(\sigma_{\text{total}})_{\bar{p}\text{-}n} - (\sigma_{\text{total}})_{\bar{p}\text{-}p}\right]^2$$

where k is the wave number of the incident antiproton in the laboratory system. This expression is derived in Appendix II. If we assume the value for the charge-exchange cross section at 0° stated above, then the difference between the total antiproton-proton and the antiproton-neutron cross sections at 440 Mev must be less than 50 mb. The $\bar{p}$-p and $\bar{p}$-n cross sections quoted in References 8 and 9 are consistent with this prediction.

ACKNOWLEDGMENTS

I am grateful to Professors Owen Chamberlain and Emilio Segrè for their guidance throughout the planning and execution of this experiment. I am indepted to Drs. Clyde Wiegand, Herbert Steiner, and Thomas Ypsilantis for many valuable discussions.

Mr. Tommy Elioff and other members of our group contributed generously of their time in the construction of the antineutron counter. The successful operation of the magnetic mass spectrograph was due largely to Messrs. Lewis Agnew and Ernie Rogers. Drs. Donald Keller and Ronald Mermod made important contributions to the success of this experiment. Finally, I would like to thank Miss Janice Button and Messrs. James Foote and Rudolf Larsen for their part in this work.

I also wish to thank Dr. Edward J. Lofgren and the staff at the Bevatron for their cooperation in the execution of this experiment.

This work was performed under the auspices of the U. S. Atomic Energy Commission.

APPENDIX

I. Pion Production in the Charge-Exchange Reaction

In this section we are concerned with a calculation of the ratio of the rate of charge exchange without pion production to the rate of the process that is the same except that it involves also the formation of a single pion. We will follow a statistical method due to Fermi[15] in computing this ratio. Both neutrons and protons are here denoted by N. Our usual notation ($\bar{p}$ and $\bar{n}$) will be used to refer to antiprotons and antineutrons. Pions are denoted by the symbol π, irrespective of their charge. We are concerned with the following two types of antiproton charge exchange:

(a) zero-pion formation: $\bar{p} + N_1 \rightarrow \bar{n} + N_2$;

(b) one-pion formation: $\bar{p} + N_1 \rightarrow \bar{n} + N_2 + \pi$.

The collision of two energetic particles may lead to the formation of several possible final states with different particle multiplicities (subject, of course, to the conservation laws). Fermi's statistical theory of particle production is based on the assumption that the probability of formation of any one of these final states depends only on its statistical weight. If spin is neglected, the statistical weight of the nucleon-antineutron final state in Process (a) is given by

$$S(2) = Vp^2/4\pi^2\hbar^3 v,$$

where p and v are the momentum and velocity of either particle in the center-of-mass system; V is the volume in which the interaction takes place, and is determined by the radius of the pion cloud surrounding the nucleon or antinucleon. If relativistic effects are neglected we have

$$V = (4/3)\pi R^3,$$

where

$$R = \hbar/\mu c$$

and μ is the pion mass.

For Reaction (b) the expression for the statistical weight is more involved because there are three particles in the final state. Assuming that these particles are nonrelativistic, Fermi[15] obtains

$$S(3) = M^3V^2/128\pi^3\hbar^6 \cdot T^2/(1/4 + M/2\mu)^{3/2} .$$

Here T is the kinetic energy available in the center of mass to the final three particles, M is the nucleon mass, and V is the interaction volume given above.

In this theory, therefore, the ratio of the probability of Process (a) to that of (b) is given by

$$S(2)/S(3) = 32\pi\hbar^3p^2 (1/4 + M/2\mu)^{3/2} \Big/ M^3VT^2v .$$

Substituting $V = (4/3)\pi (\hbar/\mu c)^3$, we obtain

$$S(2)/S(3) = (24p^2c^2/T^2)(c/v)(\mu/M)^3(1/4 + M/2\mu)^{3/2} \cong 60$$

for incident antiprotons of 440 Mev energy. This ratio favors Reaction (a) over (b) and, to the extent that these processes lie within the scope of a statistical treatment, indicates that antiproton charge exchange without pion production predominates over charge exchange that involves also the formation of a single pion.

II. Charge Independence and Its Consequences on the Nucleon-Antinucleon System

We assume charge independence and denote the total isotopic spin operator as $\vec{T}$ with a z component, T_3. The eigen values of these operators are designated by $\vec{t}$ and t_3, respectively. The t_3 components for the proton, neutron, antiproton, and antineutron are given in Table VI. The rule for the composition of the z components of isotopic spin for a system of particles and antiparticles is given by Malenka and Primakoff[16] as

$$t_3 = t_3 \text{ (particles)} + t_3 \text{ (antiparticles)}.$$

With this formalism we may construct the isotopic spin eigenfunctions for the antiproton-neutron, antiproton-proton, and antineutron-neutron systems. The state describing the $\bar{p}$-n system is pure triplet ($t_3 = -1$). The $\bar{p}$-p and $\bar{n}$-n configurations are mixtures of singlet and triplet isotopic spin states. These eigenfunctions are given in Table VI.

We are concerned with the following elastic scattering processes:

$$\bar{p} + n \rightarrow \bar{p} + n , \qquad \text{(A1)}$$

$$\bar{p} + p \rightarrow \bar{p} + p , \qquad \text{(A2)}$$

$$\bar{p} + p \rightarrow \bar{n} + n. \qquad \text{(A3)}$$

With each of these processes may be associated a scattering amplitude f which is related to the differential cross section in the usual way,

$$d\sigma/d\Omega = |f|^2 , \qquad \text{(A4)}$$

where σ is the elastic scattering cross section. We also make use of a relationship between the imaginary part of the forward-scattering amplitude $f(0^\circ)$ and the <u>total</u> cross section,[17]

$$\sigma^t = (4\pi/k) \text{ Im } f(0^\circ) , \qquad \text{(A5)}$$

where k is the wave number of the incident particle in the laboratory system.

The nucleon-antinucleon scattering amplitudes for the three scattering processes under consideration may be expressed in terms of the scattering amplitudes f_1 and f_0 for the nucleon-antinucleon

Table VI

Isotopic spin eigenfunctions and eigenvalues of T_3 for the proton, neutron, antiproton, antineutron, and certain nucleon-antinucleon systems. The superscripts on the eigenfunctions N are the z components of isotopic spin, and the subscripts are the magnitude of this vector for each case.

	p	n	$\bar{p}$	$\bar{n}$	$\bar{p}$-n	$\bar{p}$-p	$\bar{n}$-n
t_3	1/2	-1/2	-1/2	1/2	-1	0	0
Eigenfunction	$N^{1/2}_{1/2}$	$N^{-1/2}_{1/2}$	$\bar{N}^{-1/2}_{1/2}$	$\bar{N}^{-1/2}_{1/2}$	N^{-1}_{1}	$\frac{1}{\sqrt{2}}(N^0_1+N^0_0)$	$\frac{1}{\sqrt{2}}(N^0_1-N^0_0)$

isotopic triplet and singlet states, respectively. Using Table VI, we obtain

$$f_{\bar{p}n \to \bar{p}n} = f_1 , \tag{A6}$$

$$f_{\bar{p}p \to \bar{p}p} = \frac{1}{2} f_1 + \frac{1}{2} f_0 , \tag{A7}$$

$$f_{\bar{p}p \to \bar{n}n} = \frac{1}{2} f_1 - \frac{1}{2} f_0 . \tag{A8}$$

Adding Relations (A7) and (A8), we see that we have

$$f_{\bar{p}n \to \bar{p}n} = f_{\bar{p}p \to \bar{p}p} + f_{\bar{p}p \to \bar{n}n}$$

or

$$f_{\bar{p}p \to \bar{n}n} = f_{\bar{p}n \to \bar{p}n} - f_{\bar{p}p \to \bar{p}p} .$$

Taking the imaginary part of each term in this expression and evaluating at $\theta = 0^\circ$, we obtain

$$\text{Im } f_{\bar{p}p \to \bar{n}n}(0^\circ) = \text{Im } f_{\bar{p}n \to \bar{p}n}(0^\circ) - \text{Im } f_{\bar{p}p \to \bar{p}p}(0^\circ) .$$

Using the relationship given in Eq. (A5), we find

$$\text{Im } f_{\bar{p}p \to \bar{n}n}(0^\circ) = \frac{k}{4\pi} \left[\sigma^t_{\bar{p}n} - \sigma^t_{\bar{p}p} \right] , \tag{A9}$$

where $\sigma^t_{\bar{p}n}$ and $\sigma^t_{\bar{p}p}$ are the total antiproton-neutron and antiproton-proton cross sections, respectively. From the relationship expressed in Eq. (A4), we obtain

$$\left(\frac{d\sigma}{d\Omega} \right)_{\bar{p}p \to \bar{n}n} (0^\circ) \geq \left[\text{Im } f_{\bar{p}p \to \bar{n}n}(0^\circ) \right]^2 .$$

Comparison with Eq. (A9) yields the result; namely

$$\left(\frac{d\sigma}{d\Omega} \right)_{\bar{p}p \to \bar{n}n} (0^\circ) \geq \left(\frac{k}{4\pi} \right)^2 \left[\sigma^t_{\bar{p}n} - \sigma^t_{\bar{p}p} \right]^2 .$$

BIBLIOGRAPHY

1. Chamberlain, Segrè, Wiegand, and Ypsilantis, Nature 177, 11 (1956).
2. Cork, Lambertson, Piccioni, and Wenzel, Phys. Rev. 104, 1193 (1956).
3. Chamberlain, Segrè, Wiegand, and Ypsilantis, Phys. Rev. 100, 947 (1955).
4. V. L. Fitch, Bull. Am. Phys. Soc. Ser 11, 1, No. 1, 52 (1956), invited paper.
5. O. Chamberlain and C. Wiegand, "The Velocity-Selecting Cerenkov Counter," in Proceedings of the CERN Symposium on High-Energy Accelerators and Pion Physics, Vol. 2 (CERN, Geneva 1956).
6. Barkas, Birge, Chupp, Ekspong, G. Goldhaber, S. Goldhaber, Heckman, Perkins, Sandweiss, Segrè, Smith, Stork, Van Rossum and Amaldi, Baroni, Castagnoli, Franzinetti, and Manfredini, Phys. Rev. 105, 1037 (1957).
7. Edward Gross, The Absolute Yield of Low-Energy Neutrons from 190-Mev Proton Bombardment of Gold, Silver, Nickel, Aluminum, and Carbon, UCRL-3330, Feb. 1956.
8. Chamberlain, Keller, Mermod, Segrè, Steiner, and Ypsilantis, (Phys. Rev. to be publishes).
9. Agnew, Chamberlain, Keller, Mermod, Rogers, Steiner, and Wiegand, Phys. Rev. (to be published).
10. N. C. Francis and K. M. Watson, Am. J. Phys. 21, 659 (1953).
11. R. Hofstader, Rev. Mod. Phys. 28, 214 (1956).
12. R. W. Williams, Phys. Rev. 98, 1387 (1955).
13. R. C. P. Voss and R. Wilson, Phys. Rev. 99, 1056 (1955).
14. O. Miyatake and C. Goodman, Phys. Rev. 99, 1040 (1955).
15. E. Fermi, Elementary Particles Yale University Press, (New Haven, 1951), Ch. IV, p. 79.
16. B. J. Malenka and H. Primakoff, Phys. Rev. 105, 338 (1957).
17. This expression is derived for the special case of $\ell = 0$ in Fermi's lecture notes, Nuclear Physics, compiled by J. Orear, A. Rosenfeld, and R. Schluter, (University of Chicago Press, Chicago, Ill., 1950). See p. 195.
17. Hartzler, Siegel, and Opitz, Phys. Rev. 95, 591 (1954).